



CERN-EP-2023-043

16 March 2023

Data-driven precision determination of the material budget in ALICE

ALICE Collaboration*

Abstract

The knowledge of the material budget with a high precision is fundamental for measurements of direct photon production using the photon conversion method due to its direct impact on the total systematic uncertainty. Moreover, it influences many aspects of the charged-particle reconstruction performance. In this article, two procedures to determine data-driven corrections to the material-budget description in ALICE simulation software are developed. One is based on the precise knowledge of the gas composition in the Time Projection Chamber. The other is based on the robustness of the ratio between the produced number of photons and charged particles, to a large extent due to the approximate isospin symmetry in the number of produced neutral and charged pions. Both methods are applied to ALICE data allowing for a reduction of the overall material budget systematic uncertainty from 4.5% down to 2.5%. Using these methods, a locally correct material budget is also achieved. The two proposed methods are generic and can be applied to any experiment in a similar fashion.

arXiv:2303.15317v1 [physics.ins-det] 23 Mar 2023

© 2023 CERN for the benefit of the ALICE Collaboration.

Reproduction of this article or parts of it is allowed as specified in the CC-BY-4.0 license.

*See Appendix A for the list of collaboration members

1 Introduction

The ALICE experiment is a dedicated heavy-ion experiment at the CERN LHC [1–3]. In ALICE, photons are measured using either the calorimeters (PHOS [4, 5], EMCal [6–8]), or the Photon Conversion Method (PCM) [2, 9], i.e. via the reconstruction of e^+e^- pairs from photon conversions in the detector material. The material budget is, expressed in % of radiation lengths, $X/X_0 = (11.4 \pm 0.5)\%$ [2, 9]¹. This value is an average over the pseudorapidity range $|\eta| < 0.9$ and it is integrated in the radial direction (R) up to 180 cm, where R is calculated in the transverse xy -plane to the beam axis (z). This uncertainty in the material budget translates into a systematic uncertainty of photon spectrum measurements. For example, direct-photon production² was measured in Pb–Pb collisions at a center of mass energy per nucleon pair of $\sqrt{s_{NN}} = 2.76$ TeV in three centrality classes by ALICE [10]. The measurement was done by a combination of the independent PCM and PHOS measurements. A low transverse momentum (p_T) excess with respect to perturbative Quantum Chromodynamics (pQCD) prompt-photon predictions is observed, which can be attributed to thermal photon emission from the quark–gluon plasma (QGP). The current uncertainties do not allow for discrimination among the proposed theoretical models [11–19]. For the events in the 0–20% centrality interval, the low p_T excess is of the order of 10–15%, and the total uncertainty is approximately 6% at low p_T with the largest contribution being the 4.5% of the material budget. Therefore, reducing the uncertainty of the material budget is essential for improving the significance of the direct-photon measurements and, thereby, allowing for a larger discrimination power among the different theoretical models.

The estimated systematic uncertainty related to the material budget of $\pm 4.5\%$ [2, 9] is an average over the R range given above. Initially, the systematic uncertainty was estimated by comparing the reconstructed number of γ conversions (N_γ) normalized to the number of charged particles (N_γ/N_{ch}) between real data (RD) and Monte Carlo (MC) simulations. Two event generators (PYTHIA 6 [20] and PHOJET 1.12 [21]), two secondary vertex finder algorithms with different optimization criteria, and two momentum ranges were considered. Local differences of up to 20% were observed in some parts of the detector. The development of new procedures to reduce the systematic uncertainty and to achieve a more accurate local description of the material budget in the simulation is therefore mandatory.

This article establishes two data-driven correction methods for a precise determination of the material budget of a given detector using reconstructed photon conversions. The methods are based either on the existence of a well-known piece of material (e.g. the TPC gas in the ALICE case) or on the robustness of the ratio N_γ/N_{ch} above a low p_T threshold which is largely due to the approximate isospin symmetry in pion production. The two methods are developed for the ALICE experiment but can, in principle, be employed in any other experiment.

This article is organized as follows. The ALICE experimental setup and event sample used in this article and the photon reconstruction are described in Sec. 2, and Sec. 3, respectively. The proposed correction procedures are introduced in Sec. 4. The results are presented in Sec. 5 followed by the conclusions in Sec. 6.

2 Detector description and data sample

A comprehensive description of the ALICE experiment during the LHC Runs 1 and 2 and its performance can be found in Refs. [1, 2]. The relevant detectors for this analysis are the Inner Tracking System (ITS) [22], the Time Projection Chamber (TPC) [23] and the V0 detectors [24] which are operated inside

¹Obtained from the geometrical model of the ALICE experiment implemented in the simulation software.

²The terminology used for the different photon sources is as follows. Direct photons: all photons except from neutral meson decays. Thermal photons: photons from the QGP and hadron gas that are dominant at low transverse momentum ($p_T < 3$ GeV/ c). Prompt photons: produced in hard scatterings (calculable with pQCD) and pre-equilibrium photons that are dominant at high p_T ($p_T > 5$ GeV/ c).

a magnetic field up to 0.5 T directed parallel to the beam axis. The ITS consists of six cylindrical layers of high resolution silicon tracking detectors. The two innermost layers located at a radial distance of 3.9 cm and 7.6 cm are silicon pixel detectors (SPD); the two intermediate layers are silicon drift detectors (SDD) positioned at 15.0 cm and at 23.9 cm; and the two outermost layers are silicon strip detectors (SSD) at 38.0 cm and 43.0 cm. It measures the position of the primary collision vertex, the impact parameter of the tracks, and improves considerably the track p_T resolution at high p_T . The SDD and SSD layers provide the amplitude of the charged signal that is used for particle identification through the measurement of the specific energy loss (dE/dx). The TPC is a large ($\sim 85 \text{ m}^3$) cylindrical drift detector filled during 2017 with a Ne/CO₂/N₂ (90/10/5) gas mixture. It covers a pseudorapidity acceptance of $|\eta| < 0.9$ over the full azimuthal range, with a maximum of 159 reconstructed space points along the path of the track. In addition to the space points for the track reconstruction, the TPC provides particle identification via the measurement of the dE/dx . The V0 detector, which is made of two arrays of 32 plastic scintillators located at $2.8 < \eta < 5.1$ (V0A) and $-3.7 < \eta < -1.7$ (V0C), is used for triggering on the collisions [24].

The analyses presented here use the low intensity part (up to few hundred Hz interaction rate) of the data recorded in 2017 during the LHC pp run at $\sqrt{s} = 5.02 \text{ TeV}$. A total of about 4×10^7 pp collisions recorded with a minimum-bias (MB) trigger are used. The MB trigger was defined by signals in both V0 detectors in coincidence with a bunch crossing to minimize the contribution from diffractive interactions. Contamination from beam-induced background events, produced outside the interaction region, is removed using the timing information of the V0 detectors and taking into account the correlation between tracklets and clusters in the SPD detector [2]. The events used for the analysis are required to have a primary vertex in the fiducial region $|z| < 10 \text{ cm}$ along the beam-line direction. The primary vertex is reconstructed either using global tracks (with ITS and TPC information) or using SPD tracklets. The contamination from in-bunch pile-up events is removed offline by excluding events with multiple vertices reconstructed in the SPD [25].

In general, MC simulations use a geometrical model of the ALICE detectors, an event generator as input, and a particle transport software, GEANT3[26] in the ALICE case.

3 Photon reconstruction

Photons are reconstructed by measuring the e^+e^- pairs produced in photon conversions in the detector material. Charged tracks are reconstructed in the ALICE central barrel with the ITS [22] and the TPC [23], working together or independently. Two secondary-vertex algorithms with different optimization criteria are used in this analysis to search for oppositely-charged track pairs originating from a common (secondary) vertex, referred to as V^0 [2]. The V^0 sample consists mainly of K_S^0 , Λ , $\bar{\Lambda}$ decays and γ conversions. Selection criteria based on track quality, particle identification and the topology of a photon conversion are applied. The complete list of selection criteria is summarized in Table 1. Electrons, positrons, and photons are required to be within $|\eta| < 0.8$. In order to ensure good track quality, a minimum track transverse momentum of 50 MeV/ c and a fraction of TPC clusters over findable clusters (the number of geometrically possible clusters which can be assigned to a track) above 0.6 were required. The conversion point of the photon candidates should be inside the η acceptance and the conversion radius should be inside $0 < R < 180 \text{ cm}$ and within the limits given by the so called ‘line cut’ (see Table 1) to ensure that the photons come from the primary vertex. Electron identification and pion rejection are performed by using the specific energy loss dE/dx in the TPC. The selection and rejection criteria are based on the number of standard deviations ($n\sigma_e$ and $n\sigma_\pi$) around the electron and pion hypothesis, where σ is the standard deviation of the energy loss measurement. The remaining contamination from Λ , $\bar{\Lambda}$, and K_S^0 is further reduced using a two-dimensional selection in the (α, q_T) distribution, known as the Armenteros-Podolanski plot [27]; α is the longitudinal momentum asymmetry of positive and negative daughter tracks, defined as $\alpha = (p_L^+ - p_L^-)/(p_L^+ + p_L^-)$, and q_T is the transverse momentum of the decay particles with respect to the V^0 momentum. Conversion electrons have a preferred emission orientation

Table 1: Selection criteria applied to the V^0 sample to select photons among the different particles.

Track reconstruction	
e^\pm track p_T	$p_T > 0.05 \text{ GeV}/c$
e^\pm track η	$ \eta < 0.8$
$N_{\text{clusters}}/N_{\text{findable clusters}}$	$> 60\%$
conversion radius	$0 < R < 180 \text{ cm}$
line cut	$R > Z \times ZR_{\text{slope}} - Z_0$ with $ZR_{\text{slope}} = \tan(2 \times \arctan(\exp(-\eta_{\text{cut}})))$ where $Z_0 = 7 \text{ cm}$, $\eta_{\text{cut}} = 0.8$
Track identification	
$n\sigma_e$ TPC	$-3 < n\sigma_e < 5$
$n\sigma_\pi$ TPC	$n\sigma_\pi > 2$ for $0.25 < p < 3.5 \text{ GeV}/c$ $n\sigma_\pi > 0.5$ for $p > 3.5 \text{ GeV}/c$
Conversion γ topology	
q_T	$q_T < 0.05 \sqrt{1 - (\alpha/0.95)^2} \text{ GeV}/c$
photon fit quality	$\chi_{\text{max}}^2 = 20$
Ψ_{pair}	$ \Psi_{\text{pair}} < 0.1 (1 - \chi^2/\chi_{\text{max}}^2)$

that can be described by the angle ψ_{pair} between the plane that is perpendicular to the magnetic field (x-y plane) and the plane defined by the opening angle of the pair. A selection on ψ_{pair} together with a cut on the photon χ^2 of the Kalman filter fit [28] further suppresses the contamination from non-photonic V^0 candidates. Monte Carlo simulations show that a photon purity above 99% is achieved at all transverse momenta except in the vicinity of $p_T \sim 0.3 \text{ GeV}/c$ where it decreases to 98%. Figure 1 shows the probability that a reconstructed electron carries a certain fraction of the photon energy ($x = p_e/p_\gamma$) for photon candidates below and above a momentum of $0.4 \text{ GeV}/c$. The RD as well as reconstructed distributions from a MC simulation based on PYTHIA 8 with the Monash 2013 tune [29, 30] as input event generator are shown. Converted photons with $p > 0.4 \text{ GeV}/c$ can be reconstructed with electron fractional energies from 0 to 1, while at lower p only largely symmetric conversions are detected. Differences between the data and MC distributions are largely due to different photon momentum distributions that are not yet equalized at this stage (see Eq. (14)). A high purity in the photon sample can be inferred from the similarity of the red points (MC) and blue curves that represent only MC verified photons (Fig. 1).

Figure 2 displays the radial distribution of photon conversion vertices. The experimental data as well as reconstructed distributions from a MC simulation based on PYTHIA 8 with the Monash 2013 tune [29, 30] as input event generator are shown. The radial distribution of reconstructed conversion vertices clearly reveals the different detector structures corresponding to the ITS and TPC. The experimental distribution is compared to the one obtained from MC simulations that accounts for the time-dependent variations of the detector conditions. The main goal is to select the primary photon sample, i.e. photons coming from electromagnetic decays of neutral mesons or direct photons. Additionally, there are three types of background contributions shown in the figure that need special treatment. i) Primary e^+e^- pairs from π^0 (or η) Dalitz decays wrongly detected as conversion photons, mainly localized at radii smaller than 5 cm, can be suppressed by a minimum cut of 5 cm in the analysis. ii) Random combinatorial background, which is subtracted both in RD and MC based on the MC. iii) a 5–10% contribution of secondary photons [31] from weak decays of K_S^0 (e.g. $K_S^0 \rightarrow \pi^0 \pi^0$) and Λ ($\bar{\Lambda}$) (e.g. $\Lambda \rightarrow n\pi^0$) hadrons, and interactions in the detector material. The contribution from weak decays is estimated in the data by using a particle decay simulation called ‘‘cocktail simulation’’ [32] based on parametrizations of measured particle spectra, and in MC using the full MC information (labelled ‘True’ in Fig. 2). The contribution from interactions in the detector material is taken from MC, for both MC and real data (RD). The total secondary contribution is then subtracted from the photon sample in the data and in the MC simulated sample for each radial interval.

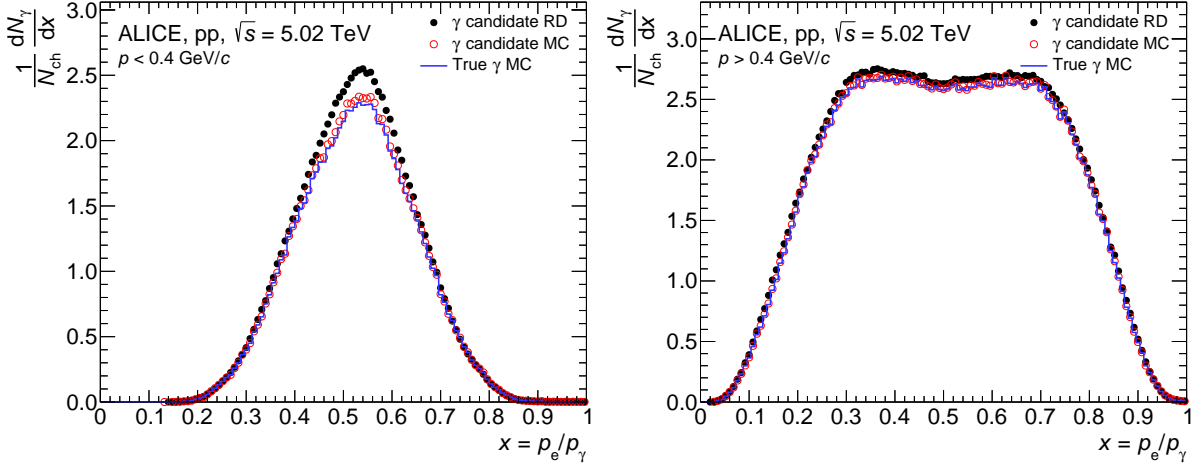


Figure 1: Distribution of the electron fractional energy (x) for photon candidates with $p < 0.4$ GeV/ c (left) and with $p > 0.4$ GeV/ c (right) reconstructed in real data (black points), in Monte Carlo simulations (red points), and for verified photons in MC simulations (blue lines) where PYTHIA8 is used as input event generator.

4 Calibration methods

The RD to MC comparison of the number of reconstructed photons as a function of the conversion point radius shown in Fig. 2 reveals local differences of up to 20% in the number of reconstructed photons³. This provides evidence that the implementation of the material budget in the geometrical model of ALICE is not accurate enough in some parts of the detector, which may impact the precision of various analyses in ALICE.

Two data-driven calibration methods (the ω_i and Ω_i calibration weights, Sec. 4.1, Sec. 4.2) were developed in order to mitigate the differences by correcting the detector material description in MC simulations, and thus, reducing the systematic uncertainty. The complete radial range is subdivided in twelve intervals as shown in Fig. 2. The resulting calibration weights are then used to scale the photon reconstruction efficiency as follows:

$$\varepsilon_{\gamma}^{\text{MC,corr}}(p_{\text{T}}) = \frac{\sum_i W_i \times dN_{\gamma,i}^{\text{rec,MC}}/dp_{\text{T}}}{dN_{\gamma}^{\text{prod}}/dp_{\text{T}}}, \quad (1)$$

where W_i are the correction factors in each radial interval i ($W_i \equiv \omega_i$ or $W_i \equiv \Omega_i$), $dN_{\gamma,i}^{\text{rec,MC}}/dp_{\text{T}}$ is the number of primary photons reconstructed in the Monte Carlo simulated data at a given p_{T} and radial interval i (see Fig. 2) in the pseudorapidity range $|\eta| < 0.8$, and $dN_{\gamma}^{\text{prod}}/dp_{\text{T}}$ is the total number of photons produced at a given p_{T} as given by the input event generator used in the MC within the same pseudorapidity interval.

Another approach for applying the calibration weights is to scale the density of the detector materials used in the geometrical model of the detector by the correction factors W_i , and produce new MC simulations. While the method given by (Eq. 1) is only valid for analyses involving photons, the scaling of the density is valid for all analyses. The only disadvantage is the need of creating new simulation samples, with the corresponding CPU needs.

4.1 TPC-gas based calibration weights: ω_i

The material-budget correction via ω_i calibration weights exploits the fact that a well-known and homogeneous part of the detector material can be used as a reference to calibrate the material budget of

³This differences could not be reduced further by checks of the ALICE geometrical model

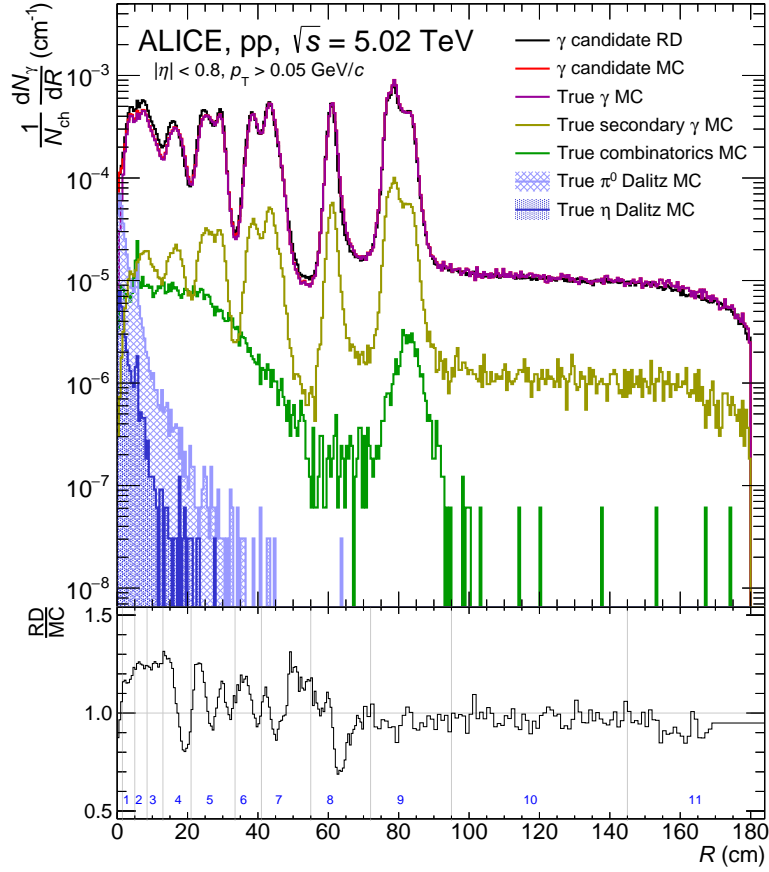


Figure 2: (Top) Radial distributions of reconstructed photon vertices in experimental data and in MC simulations are shown as black and red lines, respectively. Using the full MC information contributions from true photons (purple line), secondary photons (olive line), and combinatorial pairs (green line) are identified. The e^+e^- pairs from π^0 (or η) Dalitz decays, wrongly identified as photon conversions, are depicted as blue shaded areas. (Bottom) Ratio of the radial distribution of reconstructed photon vertices in RD (black line) and MC (red line). Vertical lines in grey and blue numbers indicate the twelve radial intervals and their respective indices used in the analysis.

the rest of the detector known with less precision. The TPC gas volume [23] in the fiducial range used for photon reconstruction, $95 < R < 145$ cm, is perfectly suited for this purpose. The TPC gas material budget depends on the exact chemical composition, temperature and pressure of the gas. During data taking, variations in the TPC gas composition and pressure are monitored with a gas chromatograph and a pressure gauge, respectively, and applied accordingly in the MC simulations via access to the conditions and calibrations database with a granularity of few hours. The temperature gradients inside the TPC are controlled to a root-mean-square (rms) deviation of less than 0.05°C [23] in order to control the drift properties. With the TPC gas monitoring system [23] the TPC gas density is known to the per mil level. The TPC-gas based calibration weights (ω_i) are then given by

$$\omega_i = \frac{N_{\gamma,i}^{\text{rec,RD}}/N_{\gamma,\text{gas}}^{\text{rec,RD}}}{N_{\gamma,i}^{\text{rec,MC}}/N_{\gamma,\text{gas}}^{\text{rec,MC}}}, \quad (2)$$

where $N_{\gamma,i}^{\text{rec,X}}$ is the number of reconstructed primary photons in a given radial interval i (denoted by ‘gas’ for the reference one) expressed as

$$N_{\gamma,i}^{\text{rec,X}} = \int_{p_{T,\text{min}}}^{\infty} \tilde{P}_i^{\text{X}}(p_T) \times \tilde{\varepsilon}_i^{\text{X}}(p_T) \frac{dN_{\gamma}^{\text{prod,X}}}{dp_T} dp_T \equiv P_i^{\text{X}} \times \varepsilon_{\gamma,i}^{\text{X}} \times N_{\gamma}^{\text{prod,X}}, \quad (3)$$

where X refers both to RD and to MC, $p_{T,\min} = 0.05$ GeV/c, N_γ^{prod} is the number of produced primary photons either in RD or in MC. The photon conversion probability, and the photon reconstruction efficiency in a given radial interval i are denoted by P_i and $\varepsilon_{\gamma,i}$, respectively. The reweighted $N_{\gamma,i}^{\text{rec}}$ is defined later in Eq. (13). The photon reconstruction efficiency is calculated using MC simulations. The RD and MC labels are also used in the efficiency to emphasize possible differences of the RD efficiency compared to the values obtained in the MC simulations. The ratio between two radial intervals suppresses the impact of different numbers of produced photons, or the overall reconstruction efficiency, between data and Monte Carlo simulations.

4.2 Pion-isospin-symmetry based calibration weights: Ω_i

The material budget correction via the Ω_i calibration weights exploits the robustness of the ratio of the number of reconstructed photons to the number of reconstructed charged particles ($N_\gamma^{\text{rec}}/N_{\text{ch}}^{\text{rec}}$) above a certain low p_T threshold. The reason for the robustness is the approximate isospin symmetry [33] in the number of produced charged and neutral pions, and that charged pions and photons from π^0 decays are the dominant contributions to the number of charged particles (90% of charged particles are charged pions) [34, 35] and the total number of photons [32], respectively. 'Approximate' is used to point out that electromagnetic decays of the η , ω and η' mesons are cases that violate the pion isospin symmetry. By employing PYTHIA 8 and PHOJET [21] event generators it was checked that the ratio is constant at the per mil level even if the charged-particle multiplicity or the photon multiplicity differ by 10–20% depending on the collision energy and event generator. In summary, the ratio of the number of reconstructed primary photons in a given radial interval ($N_{\gamma,i}^{\text{rec}}$) divided by the number of reconstructed primary charged particles (N_{ch}) in RD over the same quantity in MC (Ω_i) is sensitive to the correctness of the detector material implementation; thus, the Ω_i can be used as calibration weights.

The pion-isospin-symmetry based calibration weights (Ω_i) are then defined as

$$\Omega_i = \frac{N_{\gamma,i}^{\text{rec,RD}}/N_{\text{ch}}^{\text{rec,RD}}}{N_{\gamma,i}^{\text{rec,MC}}/N_{\text{ch}}^{\text{rec,MC}}}, \quad (4)$$

where ($N_{\text{ch}}^{\text{rec,X}}$) is the number of reconstructed primary tracks with a transverse momentum $p_T > 0.15$ GeV/c in the pseudorapidity range $|\eta| < 0.8$, X refers to RD or to MC, and $N_{\gamma,i}^{\text{rec}}$ is the number of reconstructed primary photons in the radial interval i with transverse momentum above a minimum value of 0.05 GeV/c (see Eq. (3)). The reweighted $N_{\gamma,i}^{\text{rec}}$ is defined later in Eq. (13). Charged tracks are selected with selections on the number of space points used for tracking and on the quality of the track fit, as well as on the distance of closest approach to the reconstructed vertex [35]. The contribution of secondary charged particles is subtracted in the case of data using the measurement performed in ALICE in the same data set [35], and in MC using the full MC information. The normalization to N_{ch} minimizes the impact of the model dependence of a given inclusive photon production yield N_γ^{prod} in an event generator relative to RD.

4.3 Comparison of the two calibration methods

The comparison of the two calibration factors described in Sec. 4.1 and Sec. 4.2 carries very valuable information. In order to gain insights into potential differences between the two sets of correction factors, it is useful to write them in terms of the conversion probability P_i in a given radial interval.

Taking into account Eq. (3), the ω_i calculation given by Eq. (2) transforms into

$$\omega_i = \frac{P_i^{\text{RD}} \times \varepsilon_{\gamma,i}^{\text{RD}}}{P_i^{\text{MC}} \times \varepsilon_{\gamma,i}^{\text{MC}}} \times \frac{P_{\text{gas}}^{\text{MC}} \times \varepsilon_{\gamma,\text{gas}}^{\text{MC}}}{P_{\text{gas}}^{\text{RD}} \times \varepsilon_{\gamma,\text{gas}}^{\text{RD}}}. \quad (5)$$

Under the assumption that the gas is a well-known material, the conversion probabilities in MC and RD agree for the reference radial interval, i.e.

$$P_{\text{gas}}^{\text{RD}} = P_{\text{gas}}^{\text{MC}}. \quad (6)$$

Then, the ω_i calculation given by Eq. (5) reduces to

$$\omega_i = \frac{P_i^{\text{RD}} \times \epsilon_{\gamma,i}^{\text{RD}} \times \epsilon_{\gamma,\text{gas}}^{\text{MC}}}{P_i^{\text{MC}} \times \epsilon_{\gamma,i}^{\text{MC}} \times \epsilon_{\gamma,\text{gas}}^{\text{RD}}}, \quad (7)$$

For the pion-isospin-symmetry based calibration method, Ω_i , the number of reconstructed primary charged particles (N_{ch}) in the same $|\eta|$ range is also needed:

$$N_{\text{ch}}^{\text{rec},X} = N_{\text{ch}}^{\text{prod},X} \times \epsilon_{\text{track}}^X, \quad (8)$$

where X refers to RD or MC.

Using Eq. (4) and Eq. (8) the Ω_i are given by

$$\Omega_i = \frac{P_i^{\text{RD}} \times \epsilon_{\gamma,i}^{\text{RD}} \times \epsilon_{\text{track}}^{\text{MC}} \times N_{\gamma}^{\text{prod,RD}} / N_{\text{ch}}^{\text{prod,RD}}}{P_i^{\text{MC}} \times \epsilon_{\gamma,i}^{\text{MC}} \times \epsilon_{\text{track}}^{\text{RD}} \times N_{\gamma}^{\text{prod,MC}} / N_{\text{ch}}^{\text{prod,MC}}}. \quad (9)$$

By employing the same MC simulations with PYTHIA 8 and PHOJET as event generators it was verified that the quantity $N_{\gamma}^{\text{prod}} / N_{\text{ch}}^{\text{prod}}$ is constant within approximately 1.5% when varying $p_{\text{T,min}}$ between 0.15 GeV/c and 0.25 GeV/c. The $p_{\text{T,min}}$ value reduces the diffractive contribution that is different among the two event generators. In this work, the value for the ratio $N_{\gamma}^{\text{prod}} / N_{\text{ch}}^{\text{prod}}$ obtained from PYTHIA is assumed for RD and differences between PYTHIA and PHOJET are taken as part of the systematic uncertainties. With this assumption for the quantity $N_{\gamma}^{\text{prod}} / N_{\text{ch}}^{\text{prod}}$, the calibration weights Ω_i reduce to

$$\Omega_i = \frac{P_i^{\text{RD}} \times \epsilon_{\gamma,i}^{\text{RD}} \times \epsilon_{\text{track}}^{\text{MC}}}{P_i^{\text{MC}} \times \epsilon_{\gamma,i}^{\text{MC}} \times \epsilon_{\text{track}}^{\text{RD}}}. \quad (10)$$

In case a constant (p_{T} and R -independent) factor between the V^0 reconstruction efficiencies in RD and MC would exist ($\epsilon_{\gamma,i}^{\text{RD}} / \epsilon_{\gamma,i}^{\text{MC}}$) it would drop out for the ω_i weights (see Eq. (5)). According to Eq. (10) this is not the case for Ω_i weights.

Using Eq. (5) or Eq. (7) and Eq. (10), the ratio Ω_i / ω_i is given by

$$\frac{\Omega_i}{\omega_i} = \frac{P_{\text{gas}}^{\text{RD}} \times \epsilon_{\gamma,\text{gas}}^{\text{RD}} \times \epsilon_{\text{track}}^{\text{MC}}}{P_{\text{gas}}^{\text{MC}} \times \epsilon_{\gamma,\text{gas}}^{\text{MC}} \times \epsilon_{\text{track}}^{\text{RD}}}, \quad (11)$$

or

$$\frac{\Omega_i}{\omega_i} = \frac{\epsilon_{\gamma,\text{gas}}^{\text{RD}} \times \epsilon_{\text{track}}^{\text{MC}}}{\epsilon_{\gamma,\text{gas}}^{\text{MC}} \times \epsilon_{\text{track}}^{\text{RD}}}. \quad (12)$$

By calculating the Ω_i / ω_i ratio one can cross-check if the ratio $\epsilon_{\gamma,\text{gas}} / \epsilon_{\text{track}}$, i.e. the reconstruction efficiency in the reference radial interval ‘gas’ over the charged particle reconstruction efficiency, is reproduced in MC. In case $\Omega_i / \omega_i \neq 1$, the ω_i calibration weights cannot be used directly as correction factors.

5 Determination of ω_i and Ω_i

All quantities that are needed to compute the ω_i and Ω_i correction factors are introduced in Sec. 4. The calculation of the ω_i and Ω_i weights follows an iterative procedure because, as the photon reconstruction efficiency is different for the various radial intervals, the differences between the reconstructed number of photons in RD and in MC can also result from a deviation of the shape of the MC photon p_T spectrum from RD. In order to take this effect into account, the shape of the MC simulated photon transverse momentum spectrum is adjusted to the measured shape in RD by applying weights ($\Theta(p_T)$) to the MC simulated data as

$$dN'_{\gamma}{}^{\text{rec,MC}}/dp_T = dN_{\gamma}{}^{\text{rec,MC}}/dp_T \times \Theta(p_T), \quad (13)$$

where $\Theta(p_T)$ is defined as

$$\Theta(p_T) = \frac{N_{\gamma}{}^{\text{rec,MC}}}{N_{\gamma}{}^{\text{rec,RD}}} \times \frac{dN_{\gamma}{}^{\text{rec,RD}}/dp_T}{dN_{\gamma}{}^{\text{rec,MC}}/dp_T}. \quad (14)$$

The total number of photons is preserved as only the shape of the spectrum is modified,

$$N'_{\gamma}{}^{\text{rec,MC}} = N_{\gamma}{}^{\text{rec,MC}}. \quad (15)$$

The first step is to align the shape of the reconstructed transverse momentum distributions of the MC to the data (Eq. (13)) using the $\Theta(p_T)$ factors given in Eq. (14). This step is performed twice to achieve good agreement. A set of ω_i and Ω_i is then obtained using Eq. (2) and Eq. (4), respectively. Applying the Ω_i calibration weights results in a modification of the reconstructed transverse momentum distribution. Therefore, a second iteration of the complete procedure is performed, i.e. a new set of $\Theta(p_T)$ and Ω_i is computed. Applying this new set of Ω_i does not introduce any further change in the transverse momentum distribution, i.e. the procedure of evaluating ω_i and Ω_i weights converged.

Four combinations of input event generators and V^0 finders are tested and used for the evaluation of the systematic uncertainties. PYTHIA 8 with the Monash 2013 tune [29, 30] and PHOJET 1.12 [21], available within the DPMJET 3.0 [36] package, are used. The default combination is using PYTHIA 8 as event generator, since the Monash tune is the result of an optimization for the LHC data. For PHOJET larger differences as compared with PYTHIA 8 are observed in the simulated charged-particle multiplicity distributions compared to experimental data. Both event generators show differences in the transverse momentum spectrum with respect to experimental data. These differences are considered as part of the systematic uncertainties of the resulting material budget weights. The two V^0 finders are called “on-the-fly” and “offline”. The “on-the-fly” V^0 finder searches for V^0 candidates during the tracking procedure, when the complete detector information, down to reconstructed clusters is available. The “offline” V^0 finder searches for V^0 candidates based on reconstructed tracks, which includes their full momentum vector and uncertainty covariance matrix, but no cluster level information. Each method results in a somewhat different performance in terms of reconstruction efficiency at different radii. The “on-the-fly” V^0 finder is the default choice for the calculation of the Ω_i and ω_i calibration weights, mostly because of its significantly larger efficiency, and because the photon momenta are calculated at the conversion point. By varying the V^0 finder, uncertainties on the reconstruction efficiency and its p_T and R dependence, track selection criteria, and the secondary-vertex algorithm in itself are included. By varying the event generator, uncertainties on the robustness of N_{γ}/N_{ch} are included. An additional variation of $p_{T,\text{min}}$ from 0.05 GeV/c up to 0.2 GeV/c does not yield a sizeable difference in either of the methods.

The systematic uncertainties of the weights Ω_i are calculated according to

$$\sigma_{V^0 \text{ finder}} = |W_i^{\text{PYTHIA,on-the-fly}} - W_i^{\text{PYTHIA,offline}}|, \quad (16)$$

Table 2: Sources of the relative systematic uncertainties (%) of Ω_i and ω_i for two radial intervals. The V^0 finder category includes uncertainties on the reconstruction efficiency and its p_T and R dependence, track selection criteria, as well as two V^0 finder methods. The generator category includes uncertainties on the robustness of N_γ/N_{ch} . The total systematic uncertainty is given in the last row.

	Ω_i		ω_i	
	5 cm < R < 8.5 cm	95 cm < R < 145 cm	8.5 cm < R < 13 cm	72 cm < R < 95 cm
V^0 finder	2.74 %	2.9%	2.2%	1.83%
Generator	0.16%	2.9%	3.2 %	0.62 %
$p_{T,\min}$	Negligible	Negligible	Negligible	Negligible
σ_{sys}	2.74%	4.1%	3.8%	1.93%

$$\sigma_{\text{generator}} = |W_i^{\text{PYTHIA, on-the-fly}} - W_i^{\text{PHOJET, on-the-fly}}|, \quad (17)$$

$$\sigma_{\text{sys}}^2(W_i) = \sigma_{V^0 \text{ finder}}^2(W_i) + \sigma_{\text{generator}}^2(W_i), \quad (18)$$

where $W_i \equiv \omega_i$ or $W_i \equiv \Omega_i$. Table 5 shows details for two selected radial intervals.

The radially averaged weight $\langle \Omega \rangle$ is given by

$$\langle \Omega \rangle = \sum_i \frac{N_\gamma^i}{N_\gamma^{\text{total}}} \times \Omega_i, \quad (19)$$

and, assuming that the statistical uncertainties are negligible and the systematic uncertainties are correlated among the different radial intervals, its uncertainty $\sigma(\Omega)$ is given by

$$\sigma(\Omega) = \sum_i \frac{N_\gamma^i}{N_\gamma^{\text{total}}} \times \sigma(\Omega_i). \quad (20)$$

The final set of ω_i and Ω_i calibration weights is presented in Fig. 3. The calibration weights range from a minimum value of 0.926 ± 0.034 to a maximum of 1.240 ± 0.034 , corresponding to the TPC inner containment vessel (interval 8) and the silicon pixels plus thermal shield (interval 2), respectively. The two sets of calibration weights, Ω_i and ω_i , are very similar to each other, differing by only about 2.5%. On the other hand, one observes that for $R < 55$ cm the uncertainties of Ω_i are smaller than for ω_i , while they are larger for $R > 55$ cm. The reason is that in the case of ω_i the uncertainties in the gas add to the corresponding ones in the given interval for $R < 55$ cm because the mean momentum of the reconstructed photons in radial intervals "gas" and "i" are different, while, as the radial interval comes closer to the one in the gas ($R > 55$ cm), part of the uncertainties cancels out. According to Eq. (12), a difference in the ratio can be attributed to small differences in the reconstruction efficiency ratio ($\epsilon_{\gamma,\text{gas}}/\epsilon_{\text{track}}$) in RD with respect to the one obtained in the MC simulations, or even differences in the reference calibration material (P_{gas} , see Eq. (11)). As a small difference of 2.5% is observed, the ω_i correction factors cannot be taken directly as material budget correction (see Sec. 4.3 and Eq. (12)). Consequently, the values of Ω_i as shown in Fig. 3 and given in Table 3 are taken as the best correction factors.

In order to further verify the correctness of the Ω_i values, π^0 measurements [9, 37–39] are carried out selecting photons in a given radial interval at a time, before and after applying the correction factors. The transverse momentum spectra of π^0 should not depend on the radial interval where the photons are reconstructed. π^0 transverse momentum spectra measured with two (or one) decay photons within

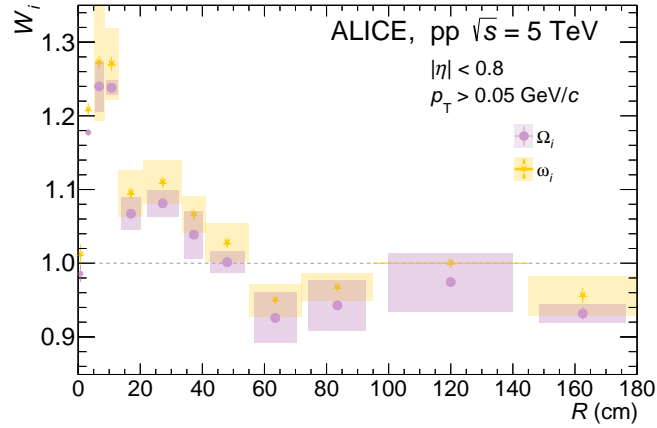


Figure 3: Distribution of the weights Ω_i and ω_i as a function of the radial position of the conversion point. Statistical uncertainties are given by the vertical bars, and systematic uncertainties are depicted by shaded areas, except for the first two intervals where only statistical uncertainties are quoted. Notice the zero ω_i systematic uncertainty in the calibration intervals ($95 \text{ cm} < R < 145 \text{ cm}$), thus an horizontal line is drawn displaying the radial interval. The width in spatial direction of the uncertainty box for the Ω_i was shrunk for better visibility.

Table 3: Correction factors Ω_i for each radial interval used in this analysis, as well as the average value. Statistical, systematic, and total uncertainties are also given, except for the first two intervals where only statistical uncertainties are quoted.

R interval	R range (cm)	Ω_i	σ_{stat} %	σ_{sys} %	σ_{total} %
0	0–1.5	0.9859	1.2	-	-
1	1.5–5	1.177	0.42	-	-
2	5–8.5	1.240	0.36	2.7	2.8
3	8.5–13	1.238	0.42	0.77	0.9
4	13–21	1.067	0.34	2.0	2.1
5	21–33.5	1.081	0.25	1.7	1.7
6	33.5–41	1.039	0.35	3.1	3.1
7	41–55	1.001	0.30	1.5	1.5
8	55–72	0.926	0.35	3.7	3.7
9	72–95	0.943	0.19	3.7	3.7
10	95–145	0.975	0.62	4.1	4.1
11	145–180	0.932	0.89	1.4	1.6
average	5–180	1.04	0.312%	2.5%	2.5%

one radial interval⁴ were analysed and compared to the spectra of charged pions [40], by fitting their ratios with a constant (see Fig. 4). The dispersion (rms) of the fit results is large when using the default MC. The fit results show clearly the same pattern as the calibration weights for the PCM-Dalitz analysis while for the PCM-PCM analysis the expected quadratic effect is observed. When using the Ω_i , the rms reduces by almost a factor 10 when both photons are reconstructed with the PCM method, or by a factor ~ 4 when only one PCM photon is used in the reconstruction, i.e., reconstructing either the Dalitz decay or reconstructing the second photon with a calorimeter. Furthermore, the ratio of the π^0 measurement in the complete radial range to the charged-pion measurement is in good agreement with the PYTHIA 8 expectations within one standard deviation.

Another observation corroborating the need for material budget correction factors is that the impact-

⁴For the Dalitz or the hybrid (PCM-EMC or PCM-PHOS) reconstruction methods, the selection of the radial interval only applies to the PCM photon.

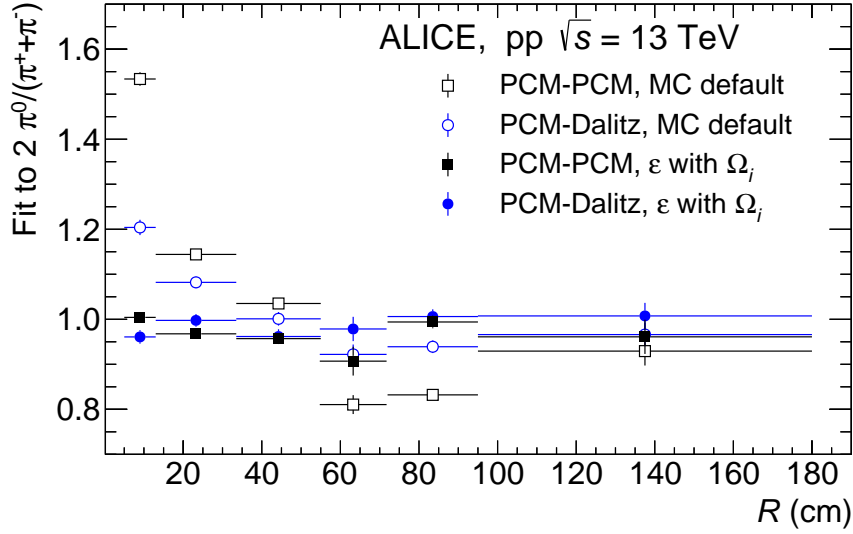


Figure 4: Zero-order polynomial fits to the ratio of neutral to charged pion transverse momentum distributions above 1 GeV/c when the two photons (PCM-PCM, $\pi^0 \rightarrow \gamma\gamma$) or one photon (PCM-Dalitz, $\pi^0 \rightarrow e^+e^-\gamma$) are selected within the given radial interval. The open symbols are obtained with efficiency corrections using the default MC, while the full symbols are obtained when the Ω_i calibration factors are used to weight the efficiency (see (Eq. 1)).

parameter resolution of charged particles, i.e., the resolution of the reconstructed distance of closest approach of a track to the primary vertex, in RD is underestimated by the default MC. The small difference between data and MC of the particle composition plays a negligible effect, as most of the charged particles are charged pions. Fig. 5 shows the impact-parameter resolution of reconstructed charged particles with a hit in the first ITS pixel layer as a function of p_T for RD and for the default MC. The difference between RD and MC is usually corrected with an ad-hoc smearing of the track parameters in the MC. On the other hand, a modified MC simulation where the correction factors as given in Table 3 are used to scale the density of the detector materials reproduces the measured resolution for $p_T < 1$ GeV/c, where the multiple scattering contribution is largest. This result confirms also that the assumption of attributing the correction factors to the material budget and not to the efficiency is correct. This demonstrates the importance of the material budget correction well beyond the reconstruction of photons with the conversion method.

6 Conclusions

Two data-driven calibration methods of the detector material description in ALICE, one based on the precise knowledge of the ALICE TPC gas and the other based on the approximate pion isospin symmetry and named ω_i and Ω_i , were developed. A reduction of the systematic uncertainty of almost a factor of two is achieved in the material budget up to a radius $R = 180$ cm corresponding approximately to the radial center of the TPC. Moreover, the differences between the description of the material distribution used for MC and the reality in the individual R intervals are mitigated. This addresses the largest source of systematic uncertainty in analyses using photon conversions. It also reduces an important, and sometimes dominant, source of systematic uncertainty in analyses based on charged-particle tracking, in particular when secondary vertices are used. The upgraded ALICE experiment for Run 3 [41] will continue to use these two calibration methods. Moreover, to assist the ω_i method, two calibrated tungsten wires were inserted in the inner and the outer barrels of ITS2 [42]. These two methods are general in nature and could be applied to any experiment in a similar fashion.

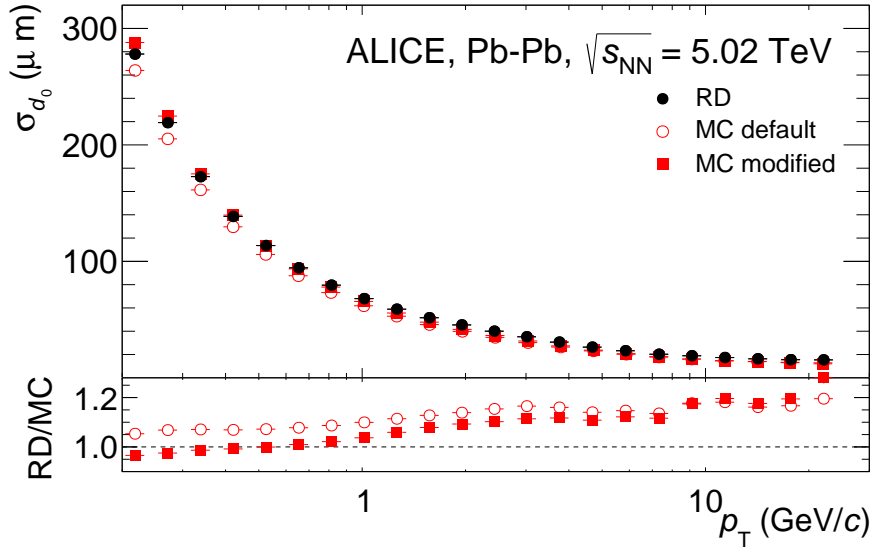


Figure 5: Top: Impact-parameter resolution of reconstructed charged particles requiring a hit in the first ITS pixel layer as a function of p_T in RD, default MC, and modified MC with the correction factors as given in Table 3. Bottom: Ratio of impact-parameter resolution to the one in the default MC (open circles) and modified MC (squares).

Acknowledgements

The ALICE Collaboration would like to thank all its engineers and technicians for their invaluable contributions to the construction of the experiment and the CERN accelerator teams for the outstanding performance of the LHC complex. The ALICE Collaboration gratefully acknowledges the resources and support provided by all Grid centres and the Worldwide LHC Computing Grid (WLCG) collaboration. The ALICE Collaboration acknowledges the following funding agencies for their support in building and running the ALICE detector: A. I. Alkhanyan National Science Laboratory (Yerevan Physics Institute) Foundation (ANSL), State Committee of Science and World Federation of Scientists (WFS), Armenia; Austrian Academy of Sciences, Austrian Science Fund (FWF): [M 2467-N36] and Nationalstiftung für Forschung, Technologie und Entwicklung, Austria; Ministry of Communications and High Technologies, National Nuclear Research Center, Azerbaijan; Conselho Nacional de Desenvolvimento Científico e Tecnológico (CNPq), Financiadora de Estudos e Projetos (Finep), Fundação de Amparo à Pesquisa do Estado de São Paulo (FAPESP) and Universidade Federal do Rio Grande do Sul (UFRGS), Brazil; Bulgarian Ministry of Education and Science, within the National Roadmap for Research Infrastructures 2020;2027 (object CERN), Bulgaria; Ministry of Education of China (MOEC), Ministry of Science & Technology of China (MSTC) and National Natural Science Foundation of China (NSFC), China; Ministry of Science and Education and Croatian Science Foundation, Croatia; Centro de Aplicaciones Tecnológicas y Desarrollo Nuclear (CEADEN), Cubaenergía, Cuba; Ministry of Education, Youth and Sports of the Czech Republic, Czech Republic; The Danish Council for Independent Research — Natural Sciences, the VILLUM FONDEN and Danish National Research Foundation (DNRF), Denmark; Helsinki Institute of Physics (HIP), Finland; Commissariat à l’Energie Atomique (CEA) and Institut National de Physique Nucléaire et de Physique des Particules (IN2P3) and Centre National de la Recherche Scientifique (CNRS), France; Bundesministerium für Bildung und Forschung (BMBF) and GSI Helmholtzzentrum für Schwerionenforschung GmbH, Germany; General Secretariat for Research and Technology, Ministry of Education, Research and Religions, Greece; National Research, Development and Innovation Office, Hungary; Department of Atomic Energy Government of India (DAE), Department of Science and Technology, Government of India (DST), University Grants Commission, Government of India (UGC) and Council of Scientific and Industrial Research (CSIR), India; National

Research and Innovation Agency - BRIN, Indonesia; Istituto Nazionale di Fisica Nucleare (INFN), Italy; Japanese Ministry of Education, Culture, Sports, Science and Technology (MEXT) and Japan Society for the Promotion of Science (JSPS) KAKENHI, Japan; Consejo Nacional de Ciencia (CONACYT) y Tecnología, through Fondo de Cooperación Internacional en Ciencia y Tecnología (FONCICYT) and Dirección General de Asuntos del Personal Académico (DGAPA), Mexico; Nederlandse Organisatie voor Wetenschappelijk Onderzoek (NWO), Netherlands; The Research Council of Norway, Norway; Commission on Science and Technology for Sustainable Development in the South (COMSATS), Pakistan; Pontificia Universidad Católica del Perú, Peru; Ministry of Education and Science, National Science Centre and WUT ID-UB, Poland; Korea Institute of Science and Technology Information and National Research Foundation of Korea (NRF), Republic of Korea; Ministry of Education and Scientific Research, Institute of Atomic Physics, Ministry of Research and Innovation and Institute of Atomic Physics and University Politehnica of Bucharest, Romania; Ministry of Education, Science, Research and Sport of the Slovak Republic, Slovakia; National Research Foundation of South Africa, South Africa; Swedish Research Council (VR) and Knut & Alice Wallenberg Foundation (KAW), Sweden; European Organization for Nuclear Research, Switzerland; Suranaree University of Technology (SUT), National Science and Technology Development Agency (NSTDA), Thailand Science Research and Innovation (TSRI) and National Science, Research and Innovation Fund (NSRF), Thailand; Turkish Energy, Nuclear and Mineral Research Agency (TENMAK), Turkey; National Academy of Sciences of Ukraine, Ukraine; Science and Technology Facilities Council (STFC), United Kingdom; National Science Foundation of the United States of America (NSF) and United States Department of Energy, Office of Nuclear Physics (DOE NP), United States of America. In addition, individual groups or members have received support from: European Research Council, Strong 2020 - Horizon 2020 (grant nos. 950692, 824093), European Union; Academy of Finland (Center of Excellence in Quark Matter) (grant nos. 346327, 346328), Finland; Programa de Apoyos para la Superación del Personal Académico, UNAM, Mexico.

References

- [1] ALICE Collaboration, K. Aamodt *et al.*, “The ALICE experiment at the CERN LHC”, *JINST* **3** (2008) S08002.
- [2] ALICE Collaboration, B. Abelev *et al.*, “Performance of the ALICE Experiment at the CERN LHC”, *Int. J. Mod. Phys. A* **29** (2014) 1430044, arXiv:1402.4476 [nucl-ex].
- [3] ALICE Collaboration, “The ALICE experiment – A journey through QCD”, arXiv:2211.04384 [nucl-ex].
- [4] ALICE Collaboration, G. Dellacasa *et al.*, “ALICE technical design report of the photon spectrometer (PHOS)”, Tech. Rep. CERN-LHCC-99-004, 1999. <https://cds.cern.ch/record/381432>.
- [5] ALICE Collaboration, S. Acharya *et al.*, “Calibration of the photon spectrometer PHOS of the ALICE experiment”, *JINST* **14** (2019) P05025, arXiv:1902.06145 [physics.ins-det].
- [6] ALICE Collaboration, P. Cortese *et al.*, “ALICE Electromagnetic Calorimeter Technical Design Report”, Tech. Rep. CERN-LHCC-2008-014, ALICE-TDR-14, 2008. <https://cds.cern.ch/record/1121574>.
- [7] J. Allen *et al.*, “ALICE DCal: An Addendum to the EMCal Technical Design Report Di-Jet and Hadron-Jet correlation measurements in ALICE”, Tech. Rep. CERN-LHCC-2010-011, ALICE-TDR-14-add-1, 2010. <https://cds.cern.ch/record/1272952>.
- [8] ALICE Collaboration, “Performance of the ALICE Electromagnetic Calorimeter”, *submitted to JINST*, arXiv:2209.04216 [physics.ins-det].

- [9] **ALICE** Collaboration, B. Abelev *et al.*, “Neutral pion and η meson production in proton-proton collisions at $\sqrt{s} = 0.9$ TeV and $\sqrt{s} = 7$ TeV”, *Phys. Lett. B* **717** (2012) 162–172, arXiv:1205.5724 [hep-ex].
- [10] **ALICE** Collaboration, J. Adam *et al.*, “Direct photon production in Pb-Pb collisions at $\sqrt{s_{NN}} = 2.76$ TeV”, *Phys. Lett. B* **754** (2016) 235–248, arXiv:1509.07324 [nucl-ex].
- [11] H. van Hees, M. He, and R. Rapp, “Pseudo-critical enhancement of thermal photons in relativistic heavy-ion collisions?”, *Nucl. Phys.* **A933** (2015) 256–271, arXiv:1404.2846 [nucl-th].
- [12] J.-F. Paquet, C. Shen, G. S. Denicol, M. Luzum, B. Schenke, S. Jeon, and C. Gale, “Production of photons in relativistic heavy-ion collisions”, *Phys. Rev.* **C93** (2016) 044906, arXiv:1509.06738 [hep-ph].
- [13] R. Chatterjee, H. Holopainen, T. Renk, and K. J. Eskola, “Collision centrality and τ_0 dependence of the emission of thermal photons from fluctuating initial state in ideal hydrodynamic calculation”, *Phys. Rev.* **C85** (2012) 064910, arXiv:1204.2249 [nucl-th].
- [14] R. Chatterjee, L. Bhattacharya, and D. K. Srivastava, “Electromagnetic probes”, *Lect. Notes Phys.* **785** (2010) 219–264, arXiv:0901.3610 [nucl-th].
- [15] O. Linnyk, V. Konchakovski, T. Steinert, W. Cassing, and E. L. Bratkovskaya, “Hadronic and partonic sources of direct photons in relativistic heavy-ion collisions”, *Phys. Rev.* **C92** (2015) 054914, arXiv:1504.05699 [nucl-th].
- [16] M. He, R. J. Fries, and R. Rapp, “Ideal Hydrodynamics for Bulk and Multistrange Hadrons in $\sqrt{s_{NN}}=200$ AGeV Au-Au Collisions”, *Phys. Rev.* **C85** (2012) 044911, arXiv:1112.5894 [nucl-th].
- [17] N. P. M. Holt, P. M. Hohler, and R. Rapp, “Thermal photon emission from the $\pi\rho\omega$ system”, *Nucl. Phys.* **A945** (2016) 1–20, arXiv:1506.09205 [hep-ph].
- [18] M. Heffernan, P. Hohler, and R. Rapp, “Universal Parametrization of Thermal Photon Rates in Hadronic Matter”, *Phys. Rev.* **C91** (2015) 027902, arXiv:1411.7012 [hep-ph].
- [19] S. Turbide, R. Rapp, and C. Gale, “Hadronic production of thermal photons”, *Phys. Rev.* **C69** (2004) 014903, arXiv:hep-ph/0308085 [hep-ph].
- [20] T. Sjostrand, S. Mrenna, and P. Z. Skands, “PYTHIA 6.4 Physics and Manual”, *JHEP* **05** (2006) 026, arXiv:hep-ph/0603175.
- [21] R. Engel, J. Ranft, and S. Roesler, “Hard diffraction in hadron hadron interactions and in photoproduction”, *Phys. Rev. D* **52** (1995) 1459–1468, arXiv:hep-ph/9502319.
- [22] **ALICE** Collaboration, K. Aamodt *et al.*, “Alignment of the ALICE Inner Tracking System with cosmic-ray tracks”, *JINST* **5** (2010) P03003, arXiv:1001.0502 [physics.ins-det].
- [23] J. Alme *et al.*, “The ALICE TPC, a large 3-dimensional tracking device with fast readout for ultra-high multiplicity events”, *Nucl. Instrum. Meth.* **A622** (2010) 316–367, arXiv:1001.1950 [physics.ins-det].
- [24] **ALICE** Collaboration, E. Abbas *et al.*, “Performance of the ALICE VZERO system”, *JINST* **8** (2013) P10016, arXiv:1306.3130 [nucl-ex].
- [25] **ALICE** Collaboration, J. Adam *et al.*, “Charged-particle multiplicities in proton–proton collisions at $\sqrt{s} = 0.9$ to 8 TeV”, *Eur. Phys. J. C* **77** (2017) 33, arXiv:1509.07541 [nucl-ex].

- [26] R. Brun, F. Bruyant, M. Maire, A. C. McPherson, and P. Zancarini, “GEANT3”, 9, 1987. CERN-DD-EE-84-1.
- [27] J. Podolanski and R. Armenteros, “III. Analysis of V-events”, *Philosophical Magazine* **45** (1954) 13–30.
- [28] I. Kisel, I. Kulakov, and M. Zyzak, “Standalone first level event selection package for the CBM experiment”, *IEEE Transactions on Nuclear Science* **60** (Oct, 2013) 3703–3708.
- [29] T. Sjöstrand, S. Ask, J. R. Christiansen, R. Corke, N. Desai, P. Ilten, S. Mrenna, S. Prestel, C. O. Rasmussen, and P. Z. Skands, “An introduction to PYTHIA 8.2”, *Comput. Phys. Commun.* **191** (2015) 159–177, arXiv:1410.3012 [hep-ph].
- [30] P. Skands, S. Carrazza, and J. Rojo, “Tuning PYTHIA 8.1: the Monash 2013 Tune”, *Eur. Phys. J. C* **74** (2014) 3024, arXiv:1404.5630 [hep-ph].
- [31] ALICE Collaboration, “The ALICE definition of primary particles”,
<https://cds.cern.ch/record/2270008>. ALICE-PUBLIC-2017-005.
- [32] ALICE Collaboration, S. Acharya *et al.*, “Direct photon production at low transverse momentum in proton-proton collisions at $\sqrt{s} = 2.76$ and 8 TeV”, *Phys. Rev.* **C99** (2019) 024912, arXiv:1803.09857 [nucl-ex].
- [33] H. Fritzsche, *Elementary particles: Building blocks of matter*. 2005.
- [34] ALICE Collaboration, S. Acharya *et al.*, “Production of charged pions, kaons, and (anti-)protons in Pb-Pb and inelastic *pp* collisions at $\sqrt{s_{NN}} = 5.02$ TeV”, *Phys. Rev. C* **101** (2020) 044907, arXiv:1910.07678 [nucl-ex].
- [35] ALICE Collaboration, S. Acharya *et al.*, “Transverse momentum spectra and nuclear modification factors of charged particles in pp, p-Pb and Pb-Pb collisions at the LHC”, *JHEP* **11** (2018) 013, arXiv:1802.09145 [nucl-ex].
- [36] S. Roesler, R. Engel, and J. Ranft, “The Monte Carlo event generator DPMJET-III”, in *International Conference on Advanced Monte Carlo for Radiation Physics, Particle Transport Simulation and Applications (MC 2000)*. 12, 2000. arXiv:hep-ph/0012252.
- [37] ALICE Collaboration, S. Acharya *et al.*, “ π^0 and η meson production in proton-proton collisions at $\sqrt{s} = 8$ TeV”, *Eur. Phys. J. C* **78** (2018) 263, arXiv:1708.08745 [hep-ex].
- [38] ALICE Collaboration, S. Acharya *et al.*, “Neutral pion and η meson production in p-Pb collisions at $\sqrt{s_{NN}} = 5.02$ TeV”, *Eur. Phys. J. C* **78** (2018) 624, arXiv:1801.07051 [nucl-ex].
- [39] ALICE Collaboration, S. Acharya *et al.*, “Neutral pion and η meson production at mid-rapidity in Pb-Pb collisions at $\sqrt{s_{NN}} = 2.76$ TeV”, *Phys. Rev. C* **98** (2018) 044901, arXiv:1803.05490 [nucl-ex].
- [40] ALICE Collaboration, S. Acharya *et al.*, “Production of light-flavor hadrons in pp collisions at $\sqrt{s} = 7$ and $\sqrt{s} = 13$ TeV”, *Eur. Phys. J. C* **81** (2021) 256, arXiv:2005.11120 [nucl-ex].
- [41] ALICE Collaboration, “ALICE upgrades during the LHC Long Shutdown 2”, arXiv:2302.01238 [physics.ins-det].
- [42] ALICE Collaboration, B. Abelev *et al.*, “Technical Design Report for the Upgrade of the ALICE Inner Tracking System”, *J. Phys. G* **41** (2014) 087002.

A The ALICE Collaboration

S. Acharya ¹²⁵, D. Adamová ⁸⁶, A. Adler⁶⁹, G. Aglieri Rinella ³², M. Agnello ²⁹, N. Agrawal ⁵⁰, Z. Ahammed ¹³², S. Ahmad ¹⁵, S.U. Ahn ⁷⁰, I. Ahuja ³⁷, A. Akindinov ¹⁴⁰, M. Al-Turany ⁹⁷, D. Aleksandrov ¹⁴⁰, B. Alessandro ⁵⁵, H.M. Alfanda ⁶, R. Alfaro Molina ⁶⁶, B. Ali ¹⁵, A. Alici ²⁵, N. Alizadehvandchali ¹¹⁴, A. Alkin ³², J. Alme ²⁰, G. Alocco ⁵¹, T. Alt ⁶³, I. Altsybeev ¹⁴⁰, M.N. Anaam ⁶, C. Andrei ⁴⁵, A. Andronic ¹³⁵, V. Anguelov⁹⁴, F. Antinori ⁵³, P. Antonioli ⁵⁰, N. Apadula ⁷⁴, L. Aphecetche ¹⁰³, H. Appelshäuser ⁶³, C. Arata ⁷³, S. Arcelli ²⁵, M. Aresti ⁵¹, R. Arnaldi ⁵⁵, J.G.M.C.A. Arneiro ¹¹⁰, I.C. Arsene ¹⁹, M. Arslanok ¹³⁷, A. Augustinus ³², R. Averbeck ⁹⁷, M.D. Azmi ¹⁵, A. Badalà ⁵², J. Bae ¹⁰⁴, Y.W. Baek ⁴⁰, X. Bai ¹¹⁸, R. Bailhache ⁶³, Y. Bailung ⁴⁷, A. Balbino ²⁹, A. Baldisseri ¹²⁸, B. Balis ², D. Banerjee ⁴, Z. Banoo ⁹¹, R. Barbera ²⁶, F. Barile ³¹, L. Barioglio ⁹⁵, M. Barlou⁷⁸, G.G. Barnaföldi ¹³⁶, L.S. Barnby ⁸⁵, V. Barret ¹²⁵, L. Barreto ¹¹⁰, C. Bartels ¹¹⁷, K. Barth ³², E. Bartsch ⁶³, N. Bastid ¹²⁵, S. Basu ⁷⁵, G. Batigne ¹⁰³, D. Battistini ⁹⁵, B. Batyunya ¹⁴¹, D. Bauri⁴⁶, J.L. Bazo Alba ¹⁰¹, I.G. Bearden ⁸³, C. Beattie ¹³⁷, P. Becht ⁹⁷, D. Behera ⁴⁷, I. Belikov ¹²⁷, A.D.C. Bell Hechavarria ¹³⁵, F. Bellini ²⁵, R. Bellwied ¹¹⁴, S. Belokurova ¹⁴⁰, G. Bencedi ¹³⁶, S. Beole ²⁴, A. Bercuci ⁴⁵, Y. Berdnikov ¹⁴⁰, A. Berdnikova ⁹⁴, L. Bergmann ⁹⁴, M.G. Besoiu ⁶², L. Betev ³², P.P. Bhaduri ¹³², A. Bhasin ⁹¹, M.A. Bhat ⁴, B. Bhattacharjee ⁴¹, L. Bianchi ²⁴, N. Bianchi ⁴⁸, J. Bielčik ³⁵, J. Bielčíková ⁸⁶, J. Biernat ¹⁰⁷, A.P. Bigot ¹²⁷, A. Bilandzic ⁹⁵, G. Biro ¹³⁶, S. Biswas ⁴, N. Bize ¹⁰³, J.T. Blair ¹⁰⁸, D. Blau ¹⁴⁰, M.B. Blidaru ⁹⁷, N. Bluhme³⁸, C. Blume ⁶³, G. Boca ^{21,54}, F. Bock ⁸⁷, T. Bodova ²⁰, A. Bogdanov¹⁴⁰, S. Boi ²², J. Bok ⁵⁷, L. Boldizsár ¹³⁶, M. Bombara ³⁷, P.M. Bond ³², G. Bonomi ^{131,54}, H. Borel ¹²⁸, A. Borissov ¹⁴⁰, H. Bossi ¹³⁷, E. Botta ²⁴, Y.E.M. Bouziani ⁶³, L. Bratrud ⁶³, P. Braun-Munzinger ⁹⁷, M. Bregant ¹¹⁰, M. Broz ³⁵, G.E. Bruno ^{96,31}, M.D. Buckland ²³, D. Budnikov¹⁴⁰, H. Buesching ⁶³, S. Bufalino ²⁹, P. Buhler ¹⁰², Z. Buthelezi ^{67,121}, A. Bylinkin ²⁰, S.A. Bysiak¹⁰⁷, M. Cai ⁶, H. Caines ¹³⁷, A. Caliva ²⁸, E. Calvo Villar ¹⁰¹, J.M.M. Camacho ¹⁰⁹, P. Camerini ²³, F.D.M. Canedo ¹¹⁰, M. Carabas ¹²⁴, A.A. Carballo ³², A.G.B. Carcamo ⁹⁴, F. Carnesecchi ³², R. Caron ¹²⁶, L.A.D. Carvalho ¹¹⁰, J. Castillo Castellanos ¹²⁸, F. Catalano ^{32,24}, C. Ceballos Sanchez ¹⁴¹, I. Chakaberia ⁷⁴, P. Chakraborty ⁴⁶, S. Chandra ¹³², S. Chapeland ³², M. Chartier ¹¹⁷, S. Chattopadhyay ¹³², S. Chattopadhyay ⁹⁹, T.G. Chavez ⁴⁴, T. Cheng ^{97,6}, C. Cheshkov ¹²⁶, B. Cheynis ¹²⁶, V. Chibante Barroso ³², D.D. Chinellato ¹¹¹, E.S. Chizzali ⁹⁵, J. Cho ⁵⁷, S. Cho ⁵⁷, P. Chochula ³², P. Christakoglou ⁸⁴, C.H. Christensen ⁸³, P. Christiansen ⁷⁵, T. Chujo ¹²³, M. Ciaccio ²⁹, C. Cicalo ⁵¹, F. Cindolo ⁵⁰, M.R. Ciupek⁹⁷, G. Clai^{II,50}, F. Colamaria ⁴⁹, J.S. Colburn¹⁰⁰, D. Colella ^{96,31}, M. Colocci ²⁵, G. Conesa Balbastre ⁷³, Z. Conesa del Valle ⁷², G. Contin ²³, J.G. Contreras ³⁵, M.L. Coquet ¹²⁸, T.M. Cormier^{1,87}, P. Cortese ^{130,55}, M.R. Cosentino ¹¹², F. Costa ³², S. Costanza ^{21,54}, C. Cot ⁷², J. Crković ⁹⁴, P. Crochet ¹²⁵, R. Cruz-Torres ⁷⁴, P. Cui ⁶, A. Dainese ⁵³, M.C. Danisch ⁹⁴, A. Danu ⁶², P. Das ⁸⁰, P. Das ⁴, S. Das ⁴, A.R. Dash ¹³⁵, S. Dash ⁴⁶, A. De Caro ²⁸, G. de Cataldo ⁴⁹, J. de Cuveland³⁸, A. De Falco ²², D. De Gruttola ²⁸, N. De Marco ⁵⁵, C. De Martin ²³, S. De Pasquale ²⁸, R. Deb¹³¹, S. Deb ⁴⁷, K.R. Deja¹³³, R. Del Grande ⁹⁵, L. Dello Stritto ²⁸, W. Deng ⁶, P. Dhankher ¹⁸, D. Di Bari ³¹, A. Di Mauro ³², B. Diab ¹²⁸, R.A. Diaz ^{141,7}, T. Dietel ¹¹³, Y. Ding ⁶, R. Divià ³², D.U. Dixit ¹⁸, Ø. Djuvsland²⁰, U. Dmitrieva ¹⁴⁰, A. Dobrin ⁶², B. Dönigus ⁶³, J.M. Dubinski¹³³, A. Dubla ⁹⁷, S. Dudi ⁹⁰, P. Dupieux ¹²⁵, M. Durkac¹⁰⁶, N. Dzalaiova¹², T.M. Eder ¹³⁵, R.J. Ehlers ⁷⁴, F. Eisenhut ⁶³, D. Elia ⁴⁹, B. Erazmus ¹⁰³, F. Ercolessi ²⁵, F. Erhardt ⁸⁹, M.R. Ersdal²⁰, B. Espagnon ⁷², G. Eulisse ³², D. Evans ¹⁰⁰, S. Evdokimov ¹⁴⁰, L. Fabbietti ⁹⁵, M. Faggin ²⁷, J. Faivre ⁷³, F. Fan⁶, W. Fan ⁷⁴, A. Fantoni ⁴⁸, M. Fasel ⁸⁷, P. Fedichio²⁹, A. Feliciello ⁵⁵, G. Feofilov ¹⁴⁰, A. Fernández Téllez ⁴⁴, L. Ferrandi ¹¹⁰, M.B. Ferrer ³², A. Ferrero ¹²⁸, C. Ferrero ⁵⁵, A. Ferretti ²⁴, V.J.G. Feuillard ⁹⁴, V. Filova³⁵, D. Finogeev ¹⁴⁰, F.M. Fionda ⁵¹, F. Flor ¹¹⁴, A.N. Flores ¹⁰⁸, S. Foertsch ⁶⁷, I. Fokin ⁹⁴, S. Fokin ¹⁴⁰, E. Fragiaco ⁵⁶, E. Frajna ¹³⁶, U. Fuchs ³², N. Funicello ²⁸, C. Furget⁷³, A. Furs ¹⁴⁰, T. Fusayasu ⁹⁸, J.J. Gaardhøje ⁸³, M. Gagliardi ²⁴, A.M. Gago ¹⁰¹, C.D. Galvan ¹⁰⁹, D.R. Gangadharan ¹¹⁴, P. Ganoti ⁷⁸, C. Garabatos ⁹⁷, J.R.A. Garcia⁴⁴, E. Garcia-Solis ⁹, C. Gargiulo ³², A. Garibli⁸¹, K. Garner¹³⁵, P. Gasik ⁹⁷, A. Gautam ¹¹⁶, M.B. Gay Ducati ⁶⁵, M. Germain ¹⁰³, A. Ghimouz¹²³, C. Ghosh¹³², M. Giacalone ^{50,25}, P. Giubellino ^{97,55}, P. Giubilato ²⁷, A.M.C. Glaenger ¹²⁸, P. Glässel ⁹⁴, E. Glimos¹²⁰, D.J.Q. Goh⁷⁶, V. Gonzalez ¹³⁴, S. Gorbunov³⁸, M. Gorgon ², K. Goswami ⁴⁷, S. Gotovac³³, V. Grabski ⁶⁶, L.K. Graczykowski ¹³³, E. Grecka ⁸⁶, A. Grelli ⁵⁸, C. Grigoras ³², V. Grigoriev¹⁴⁰, S. Grigoryan ^{141,1}, F. Grosa ³², J.F. Grosse-Oetringhaus ³², R. Grosso ⁹⁷, D. Grund ³⁵, G.G. Guardiano ¹¹¹, R. Guernane ⁷³, M. Guilbaud ¹⁰³, K. Gulbrandsen ⁸³, T. Gundem ⁶³, T. Gunji ¹²², W. Guo ⁶, A. Gupta ⁹¹, R. Gupta ⁹¹, R. Gupta ⁴⁷, S.P. Guzman⁴⁴, K. Gwizdzial ¹³³, L. Gyulai ¹³⁶,

M.K. Habib⁹⁷, C. Hadjidakis⁷², F.U. Haider⁹¹, H. Hamagaki⁷⁶, A. Hamdi⁷⁴, M. Hamid⁶, Y. Han¹³⁸, B.G. Hanley¹³⁴, R. Hannigan¹⁰⁸, J. Hansen⁷⁵, M.R. Haque¹³³, J.W. Harris¹³⁷, A. Harton⁹, H. Hassan⁸⁷, D. Hatzifotiadou⁵⁰, P. Hauer⁴², L.B. Havener¹³⁷, S.T. Heckel⁹⁵, E. Hellbär⁹⁷, H. Helstrup³⁴, M. Hemmer⁶³, T. Herman³⁵, G. Herrera Corral⁸, F. Herrmann¹³⁵, S. Herrmann¹²⁶, K.F. Hetland³⁴, B. Heybeck⁶³, H. Hillemanns³², B. Hippolyte¹²⁷, F.W. Hoffmann⁶⁹, B. Hofman⁵⁸, B. Hohlweger⁸⁴, G.H. Hong¹³⁸, M. Horst⁹⁵, A. Horzyk², Y. Hou⁶, P. Hristov³², C. Hughes¹²⁰, P. Huhn⁶³, L.M. Huhta¹¹⁵, T.J. Humanic⁸⁸, L.A. Husova¹³⁵, A. Hutson¹¹⁴, R. Ilkaev¹⁴⁰, H. Ilyas¹³, M. Inaba¹²³, G.M. Innocenti³², M. Ippolitov¹⁴⁰, A. Isakov⁸⁶, T. Isidori¹¹⁶, M.S. Islam⁹⁹, M. Ivanov¹², M. Ivanov⁹⁷, V. Ivanov¹⁴⁰, K.E. Iversen⁷⁵, M. Jablonski², B. Jacak⁷⁴, N. Jacazio²⁵, P.M. Jacobs⁷⁴, S. Jadlovská¹⁰⁶, J. Jadlovsky¹⁰⁶, S. Jaelani⁸², C. Jahnke¹¹¹, M.J. Jakubowska¹³³, M.A. Janik¹³³, T. Janson⁶⁹, M. Jercic⁸⁹, S. Ji¹⁶, S. Jia¹⁰, A.A.P. Jimenez⁶⁴, F. Jonas⁸⁷, J.M. Jowett^{32,97}, J. Jung⁶³, M. Jung⁶³, A. Junique³², A. Jusko¹⁰⁰, M.J. Kabus^{32,133}, J. Kaewjai¹⁰⁵, P. Kalinak⁵⁹, A.S. Kalteyer⁹⁷, A. Kalweit³², V. Kaplin¹⁴⁰, A. Karasu Uysal⁷¹, D. Karatovic⁸⁹, O. Karavichev¹⁴⁰, T. Karavicheva¹⁴⁰, P. Karczmarczyk¹³³, E. Karpechev¹⁴⁰, U. Keschull⁶⁹, R. Keidel¹³⁹, D.L.D. Keijdener⁵⁸, M. Keil³², B. Ketzer⁴², S.S. Khade⁴⁷, A.M. Khan⁶, S. Khan¹⁵, A. Khanzadeev¹⁴⁰, Y. Kharlov¹⁴⁰, A. Khatun¹¹⁶, A. Khuntia¹⁰⁷, M.B. Kidson¹¹³, B. Kileng³⁴, B. Kim¹⁰⁴, C. Kim¹⁶, D.J. Kim¹¹⁵, E.J. Kim⁶⁸, J. Kim¹³⁸, J.S. Kim⁴⁰, J. Kim⁵⁷, J. Kim⁶⁸, M. Kim¹⁸, S. Kim¹⁷, T. Kim¹³⁸, K. Kimura⁹², S. Kirsch⁶³, I. Kisel³⁸, S. Kiselev¹⁴⁰, A. Kisiel¹³³, J.P. Kitowski², J.L. Klay⁵, J. Klein³², S. Klein⁷⁴, C. Klein-Bösing¹³⁵, M. Kleiner⁶³, T. Klemenz⁹⁵, A. Kluge³², A.G. Knospe¹¹⁴, C. Kobdaj¹⁰⁵, T. Kollegger⁹⁷, A. Kondratyev¹⁴¹, N. Kondratyeva¹⁴⁰, E. Kondratyuk¹⁴⁰, J. König⁶³, S.A. Königstorfer⁹⁵, P.J. Konopka³², G. Kornakov¹³³, S.D. Koryciak², A. Kotliarov⁸⁶, V. Kovalenko¹⁴⁰, M. Kowalski¹⁰⁷, V. Kozuharov³⁶, I. Králik⁵⁹, A. Kravčáková³⁷, L. Krcal^{32,38}, M. Krivda^{100,59}, F. Krizek⁸⁶, K. Krizkova Gajdosova³², M. Kroesen⁹⁴, M. Krüger⁶³, D.M. Krupova³⁵, E. Kryshen¹⁴⁰, V. Kučera⁵⁷, C. Kuhn¹²⁷, P.G. Kuijter⁸⁴, T. Kumaoka¹²³, D. Kumar¹³², L. Kumar⁹⁰, N. Kumar⁹⁰, S. Kumar³¹, S. Kundu³², P. Kurashvili⁷⁹, A. Kurepin¹⁴⁰, A.B. Kurepin¹⁴⁰, A. Kuryakin¹⁴⁰, S. Kushpil⁸⁶, J. Kvapil¹⁰⁰, M.J. Kweon⁵⁷, Y. Kwon¹³⁸, S.L. La Pointe³⁸, P. La Rocca²⁶, A. Lakrathok¹⁰⁵, M. Lamanna³², R. Langoy¹¹⁹, P. Larionov³², E. Laudi³², L. Lautner^{32,95}, R. Lavicka¹⁰², R. Lea^{131,54}, L. Leardini⁹⁴, H. Lee¹⁰⁴, I. Legrand⁴⁵, G. Legras¹³⁵, J. Lehrbach³⁸, T.M. Lelek², R.C. Lemmon⁸⁵, I. León Monzón¹⁰⁹, M.M. Lesch⁹⁵, E.D. Lesser¹⁸, P. Lévai¹³⁶, X. Li¹⁰, X.L. Li⁶, J. Lien¹¹⁹, R. Lietava¹⁰⁰, I. Likmeta¹¹⁴, B. Lim²⁴, S.H. Lim¹⁶, V. Lindenstruth³⁸, A. Lindner⁴⁵, C. Lippmann⁹⁷, A. Liu¹⁸, D.H. Liu⁶, J. Liu¹¹⁷, G.S.S. Liveraro¹¹¹, I.M. Lofnes²⁰, C. Loizides⁸⁷, S. Lokos¹⁰⁷, J. Lomker⁵⁸, P. Loncar³³, J.A. Lopez⁹⁴, X. Lopez¹²⁵, E. López Torres⁷, P. Lu^{97,118}, J.R. Luhder¹³⁵, M. Lunardon²⁷, G. Luparello⁵⁶, Y.G. Ma³⁹, M. Mager³², A. Maire¹²⁷, M.V. Makariev³⁶, M. Malaev¹⁴⁰, G. Malfattore²⁵, N.M. Malik⁹¹, Q.W. Malik¹⁹, S.K. Malik⁹¹, L. Malinina^{VI,141}, D. Mallick⁸⁰, N. Mallick⁴⁷, G. Mandaglio^{30,52}, S.K. Mandal⁷⁹, V. Manko¹⁴⁰, F. Manso¹²⁵, V. Manzari⁴⁹, Y. Mao⁶, R.W. Marcjan², G.V. Margagliotti²³, A. Margotti⁵⁰, A. Marín⁹⁷, C. Markert¹⁰⁸, P. Martinengo³², M.I. Martínez⁴⁴, G. Martínez García¹⁰³, M.P.P. Martins¹¹⁰, S. Masciocchi⁹⁷, M. Masera²⁴, A. Masoni⁵¹, L. Massacrier⁷², A. Mastroserio^{129,49}, O. Matonoha⁷⁵, S. Mattiazzo²⁷, P.F.T. Matuoka¹¹⁰, A. Matyja¹⁰⁷, C. Mayer¹⁰⁷, A.L. Mazuecos³², F. Mazzaschi²⁴, M. Mazzilli³², J.E. Mdhuli¹²¹, A.F. Mechler⁶³, Y. Melikyan^{43,140}, A. Menchaca-Rocha⁶⁶, E. Meninno^{102,28}, A.S. Menon¹¹⁴, M. Meres¹², S. Mhlanga^{113,67}, Y. Miake¹²³, L. Micheletti³², L.C. Migliorin¹²⁶, D.L. Mihaylov⁹⁵, K. Mikhaylov^{141,140}, A.N. Mishra¹³⁶, D. Miśkowiec⁹⁷, A. Modak⁴, A.P. Mohanty⁵⁸, B. Mohanty⁸⁰, M. Mohisin Khan^{III,15}, M.A. Molander⁴³, Z. Moravcova⁸³, C. Mordasini⁹⁵, D.A. Moreira De Godoy¹³⁵, I. Morozov¹⁴⁰, A. Morsch³², T. Mrnjavac³², V. Muccifora⁴⁸, S. Muhuri¹³², J.D. Mulligan⁷⁴, A. Mulliri²², M.G. Munhoz¹¹⁰, R.H. Munzer⁶³, H. Murakami¹²², S. Murray¹¹³, L. Musa³², J. Musinsky⁵⁹, J.W. Myrcha¹³³, B. Naik¹²¹, A.I. Nambrath¹⁸, B.K. Nandi⁴⁶, R. Nania⁵⁰, E. Nappi⁴⁹, A.F. Nassirpour^{17,75}, A. Nath⁹⁴, C. Nattrass¹²⁰, M.N. Naydenov³⁶, A. Neagu¹⁹, A. Negru¹²⁴, L. Nellen⁶⁴, G. Neskovic³⁸, B.S. Nielsen⁸³, E.G. Nielsen⁸³, S. Nikolaev¹⁴⁰, S. Nikulin¹⁴⁰, V. Nikulin¹⁴⁰, F. Noferini⁵⁰, S. Noh¹¹, P. Nomokonov¹⁴¹, J. Norman¹¹⁷, N. Novitzky¹²³, P. Nowakowski¹³³, A. Nyanin¹⁴⁰, J. Nystrand²⁰, M. Ogino⁷⁶, A. Ohlson⁷⁵, V.A. Okorokov¹⁴⁰, J. Olienczak¹³³, A.C. Oliveira Da Silva¹²⁰, M.H. Oliver¹³⁷, A. Onnerstad¹¹⁵, C. Oppedisano⁵⁵, A. Ortiz Velasquez⁶⁴, J. Otwinowski¹⁰⁷, M. Oya⁹², K. Oyama⁷⁶, Y. Pachmayer⁹⁴, S. Padhan⁴⁶, D. Pagano^{131,54}, G. Paić⁶⁴, A. Palasciano⁴⁹, S. Panebianco¹²⁸, H. Park¹²³, H. Park¹⁰⁴, J. Park⁵⁷, J.E. Parkkila³², R.N. Patra⁹¹, B. Paul²², H. Pei⁶, T. Peitzmann⁵⁸, X. Peng⁶, M. Pennisi²⁴,

D. Peresunko ¹⁴⁰, G.M. Perez ⁷, S. Perrin ¹²⁸, Y. Pestov ¹⁴⁰, V. Petrov ¹⁴⁰, M. Petrovici ⁴⁵,
 R.P. Pezzi ^{103,65}, S. Piano ⁵⁶, M. Pikna ¹², P. Pillot ¹⁰³, O. Pinazza ^{50,32}, L. Pinsky ¹¹⁴, C. Pinto ⁹⁵,
 S. Pisano ⁴⁸, M. Płoskoń ⁷⁴, M. Planinic ⁸⁹, F. Pliquett ⁶³, M.G. Poghosyan ⁸⁷, B. Polichtchouk ¹⁴⁰,
 S. Politano ²⁹, N. Poljak ⁸⁹, A. Pop ⁴⁵, S. Porteboeuf-Houssais ¹²⁵, V. Pozdniakov ¹⁴¹, I.Y. Pozos ⁴⁴,
 K.K. Pradhan ⁴⁷, S.K. Prasad ⁴, S. Prasad ⁴⁷, R. Preghenella ⁵⁰, F. Prino ⁵⁵, C.A. Pruneau ¹³⁴,
 I. Pshenichnov ¹⁴⁰, M. Puccio ³², S. Pucillo ²⁴, Z. Pugelova ¹⁰⁶, S. Qiu ⁸⁴, L. Quaglia ²⁴,
 R.E. Quishpe ¹¹⁴, S. Ragoni ¹⁴, A. Rakotozafindrabe ¹²⁸, L. Ramello ^{130,55}, F. Rami ¹²⁷, S.A.R. Ramirez ⁴⁴,
 T.A. Rancien ⁷³, M. Rasa ²⁶, S.S. Räsänen ⁴³, R. Rath ⁵⁰, M.P. Rauch ²⁰, I. Ravasenga ⁸⁴,
 K.F. Read ^{87,120}, C. Reckziegel ¹¹², A.R. Redelbach ³⁸, K. Redlich ^{IV,79}, C.A. Reetz ⁹⁷, A. Rehman ²⁰,
 F. Reidt ³², H.A. Reme-Ness ³⁴, Z. Rescakova ³⁷, K. Reygers ⁹⁴, A. Riabov ¹⁴⁰, V. Riabov ¹⁴⁰,
 R. Ricci ²⁸, M. Richter ¹⁹, A.A. Riedel ⁹⁵, W. Riegler ³², C. Ristea ⁶², M.V. Rodriguez ³², M. Rodríguez
 Cahuantzi ⁴⁴, K. Røed ¹⁹, R. Rogalev ¹⁴⁰, E. Rogochaya ¹⁴¹, T.S. Rogoschinski ⁶³, D. Rohr ³²,
 D. Röhrich ²⁰, P.F. Rojas ⁴⁴, S. Rojas Torres ³⁵, P.S. Rokita ¹³³, G. Romanenko ¹⁴¹, F. Ronchetti ⁴⁸,
 A. Rosano ^{30,52}, E.D. Rosas ⁶⁴, K. Roslon ¹³³, A. Rossi ⁵³, A. Roy ⁴⁷, S. Roy ⁴⁶, N. Rubini ²⁵,
 O.V. Rueda ¹¹⁴, D. Ruggiano ¹³³, R. Rui ²³, P.G. Russek ², R. Russo ⁸⁴, A. Rustamov ⁸¹,
 E. Ryabinkin ¹⁴⁰, Y. Ryabov ¹⁴⁰, A. Rybicki ¹⁰⁷, H. Rytkonen ¹¹⁵, J. Ryu ¹⁶, W. Rzesza ¹³³,
 O.A.M. Saarimaki ⁴³, R. Sadek ¹⁰³, S. Sadhu ³¹, S. Sadovsky ¹⁴⁰, J. Saetre ²⁰, K. Šafařík ³⁵, P. Saha ⁴¹,
 S.K. Saha ⁴, S. Saha ⁸⁰, B. Sahoo ⁴⁶, B. Sahoo ⁴⁷, R. Sahoo ⁴⁷, S. Sahoo ⁶⁰, D. Sahu ⁴⁷, P.K. Sahu ⁶⁰,
 J. Saini ¹³², K. Sajdakova ³⁷, S. Sakai ¹²³, M.P. Salvan ⁹⁷, S. Sambyal ⁹¹, I. Sanna ^{32,95},
 T.B. Saramela ¹¹⁰, D. Sarkar ¹³⁴, N. Sarkar ¹³², P. Sarma ⁴¹, V. Sarritzu ²², V.M. Sarti ⁹⁵, M.H.P. Sas ¹³⁷,
 J. Schambach ⁸⁷, H.S. Scheid ⁶³, C. Schiaua ⁴⁵, R. Schicker ⁹⁴, A. Schmah ⁹⁴, C. Schmidt ⁹⁷,
 H.R. Schmidt ⁹³, M.O. Schmidt ³², M. Schmidt ⁹³, N.V. Schmidt ⁸⁷, A.R. Schmier ¹²⁰, R. Schotter ¹²⁷,
 A. Schröter ³⁸, J. Schukraft ³², K. Schwarz ⁹⁷, K. Schweda ⁹⁷, G. Scioli ²⁵, E. Scomparin ⁵⁵,
 J.E. Seger ¹⁴, Y. Sekiguchi ¹²², D. Sekihata ¹²², I. Selyuzhenkov ⁹⁷, S. Senyukov ¹²⁷, J.J. Seo ⁵⁷,
 D. Serebryakov ¹⁴⁰, L. Šerkšnytė ⁹⁵, A. Sevcenco ⁶², T.J. Shaba ⁶⁷, A. Shabetai ¹⁰³, R. Shahoyan ³²,
 A. Shangaraev ¹⁴⁰, A. Sharma ⁹⁰, B. Sharma ⁹¹, D. Sharma ⁴⁶, H. Sharma ^{53,107}, M. Sharma ⁹¹,
 S. Sharma ⁷⁶, S. Sharma ⁹¹, U. Sharma ⁹¹, A. Shatat ⁷², O. Sheibani ¹¹⁴, K. Shigaki ⁹², M. Shimomura ⁷⁷,
 J. Shin ¹¹, S. Shirinkin ¹⁴⁰, Q. Shou ³⁹, Y. Sibiriak ¹⁴⁰, S. Siddhanta ⁵¹, T. Siemiarczuk ⁷⁹, T.F. Silva ¹¹⁰,
 D. Silvermyr ⁷⁵, T. Simantathammakul ¹⁰⁵, R. Simeonov ³⁶, B. Singh ⁹¹, B. Singh ⁹⁵, K. Singh ⁴⁷,
 R. Singh ⁸⁰, R. Singh ⁹¹, R. Singh ⁴⁷, S. Singh ¹⁵, V.K. Singh ¹³², V. Singhal ¹³², T. Sinha ⁹⁹,
 B. Sitar ¹², M. Sitta ^{130,55}, T.B. Skaali ¹⁹, G. Skorodumovs ⁹⁴, M. Slupecki ⁴³, N. Smirnov ¹³⁷,
 R.J.M. Snellings ⁵⁸, E.H. Solheim ¹⁹, J. Song ¹¹⁴, A. Songmoonak ¹⁰⁵, C. Sonnabend ^{32,97},
 F. Soramel ²⁷, A.B. Soto-herandez ⁸⁸, R. Spijkers ⁸⁴, I. Sputowska ¹⁰⁷, J. Staa ⁷⁵, J. Stachel ⁹⁴,
 I. Stan ⁶², P.J. Steffanic ¹²⁰, S.F. Stiefelmaier ⁹⁴, D. Stocco ¹⁰³, I. Storehaug ¹⁹, P. Stratmann ¹³⁵,
 S. Strazzi ²⁵, C.P. Stylianidis ⁸⁴, A.A.P. Suaide ¹¹⁰, C. Suire ⁷², M. Sukhanov ¹⁴⁰, M. Suljic ³²,
 R. Sultanov ¹⁴⁰, V. Sumberia ⁹¹, S. Sumowidagdo ⁸², S. Swain ⁶⁰, I. Szarka ¹², M. Szymkowski ¹³³,
 S.F. Taghavi ⁹⁵, G. Tallepied ⁹⁷, J. Takahashi ¹¹¹, G.J. Tambave ⁸⁰, S. Tang ⁶, Z. Tang ¹¹⁸, J.D. Tapia
 Takaki ^{V,116}, N. Tapus ¹²⁴, M.G. Tarzila ⁴⁵, G.F. Tassielli ³¹, A. Tauro ³², G. Tejeda Muñoz ⁴⁴,
 A. Telesca ³², L. Terlizzi ²⁴, C. Terrevoli ¹¹⁴, S. Thakur ⁴, D. Thomas ¹⁰⁸, A. Tikhonov ¹⁴⁰,
 A.R. Timmins ¹¹⁴, M. Tkacik ¹⁰⁶, T. Tkacik ¹⁰⁶, A. Toia ⁶³, R. Tokumoto ⁹², N. Topilskaya ¹⁴⁰,
 M. Toppi ⁴⁸, T. Tork ⁷², A.G. Torres Ramos ³¹, A. Trifiró ^{30,52}, A.S. Triolo ^{32,30,52}, S. Tripathy ⁵⁰,
 T. Tripathy ⁴⁶, S. Trogolo ³², V. Trubnikov ³, W.H. Trzaska ¹¹⁵, T.P. Trzcinski ¹³³, A. Tumkin ¹⁴⁰,
 R. Turrisi ⁵³, T.S. Tveter ¹⁹, K. Ullaland ²⁰, B. Ulukutlu ⁹⁵, A. Uras ¹²⁶, M. Urioni ^{54,131},
 G.L. Usai ²², M. Vala ³⁷, N. Valle ²¹, L.V.R. van Doremalen ⁵⁸, M. van Leeuwen ⁸⁴, C.A. van Veen ⁹⁴,
 R.J.G. van Weelden ⁸⁴, P. Vande Vyvre ³², D. Varga ¹³⁶, Z. Varga ¹³⁶, M. Vasileiou ⁷⁸, A. Vasiliev ¹⁴⁰,
 O. Vázquez Doce ⁴⁸, V. Vechernin ¹⁴⁰, E. Vercellin ²⁴, S. Vergara Limón ⁴⁴, L. Vermunt ⁹⁷,
 R. Vértesi ¹³⁶, M. Verweij ⁵⁸, L. Vickovic ³³, Z. Vilakazi ¹²¹, O. Villalobos Baillie ¹⁰⁰, A. Villani ²³,
 G. Vino ⁴⁹, A. Vinogradov ¹⁴⁰, T. Virgili ²⁸, M.M.O. Virta ¹¹⁵, V. Vislavicius ⁷⁵, A. Vodopyanov ¹⁴¹,
 B. Volkel ³², M.A. Völkl ⁹⁴, K. Voloshin ¹⁴⁰, S.A. Voloshin ¹³⁴, G. Volpe ³¹, B. von Haller ³²,
 I. Vorobyev ⁹⁵, N. Vozniuk ¹⁴⁰, J. Vrláková ³⁷, J. Wan ³⁹, C. Wang ³⁹, D. Wang ³⁹, Y. Wang ³⁹,
 A. Wegrzynek ³², F.T. Weiglhofer ³⁸, S.C. Wenzel ³², J.P. Wessels ¹³⁵, S.L. Weyhmiller ¹³⁷,
 J. Wiechula ⁶³, J. Wikne ¹⁹, G. Wilk ⁷⁹, J. Wilkinson ⁹⁷, G.A. Willems ¹³⁵, B. Windelband ⁹⁴,
 M. Winn ¹²⁸, J.R. Wright ¹⁰⁸, W. Wu ³⁹, Y. Wu ¹¹⁸, R. Xu ⁶, A. Yadav ⁴², A.K. Yadav ¹³², S. Yalcin ⁷¹,
 Y. Yamaguchi ⁹², S. Yang ²⁰, S. Yano ⁹², Z. Yin ⁶, I.-K. Yoo ¹⁶, J.H. Yoon ⁵⁷, H. Yu ¹¹, S. Yuan ²⁰,
 A. Yuncu ⁹⁴, V. Zaccolo ²³, C. Zampolli ³², F. Zanone ⁹⁴, N. Zardoshti ³², A. Zarochentsev ¹⁴⁰,
 P. Závada ⁶¹, N. Zaviyalov ¹⁴⁰, M. Zhalov ¹⁴⁰, B. Zhang ⁶, L. Zhang ³⁹, S. Zhang ³⁹, X. Zhang ⁶,

Y. Zhang¹¹⁸, Z. Zhang⁶, M. Zhao¹⁰, V. Zhrebchevskii¹⁴⁰, Y. Zhi¹⁰, D. Zhou⁶, Y. Zhou⁸³,
J. Zhu^{97,6}, Y. Zhu⁶, S.C. Zugravel⁵⁵, N. Zurlo^{131,54}

Affiliation Notes

^I Deceased

^{II} Also at: Italian National Agency for New Technologies, Energy and Sustainable Economic Development (ENEA), Bologna, Italy

^{III} Also at: Department of Applied Physics, Aligarh Muslim University, Aligarh, India

^{IV} Also at: Institute of Theoretical Physics, University of Wroclaw, Poland

^V Also at: University of Kansas, Lawrence, Kansas, United States

^{VI} Also at: An institution covered by a cooperation agreement with CERN

Collaboration Institutes

¹ A.I. Alikhanyan National Science Laboratory (Yerevan Physics Institute) Foundation, Yerevan, Armenia

² AGH University of Science and Technology, Cracow, Poland

³ Bogolyubov Institute for Theoretical Physics, National Academy of Sciences of Ukraine, Kiev, Ukraine

⁴ Bose Institute, Department of Physics and Centre for Astroparticle Physics and Space Science (CAPSS), Kolkata, India

⁵ California Polytechnic State University, San Luis Obispo, California, United States

⁶ Central China Normal University, Wuhan, China

⁷ Centro de Aplicaciones Tecnológicas y Desarrollo Nuclear (CEADEN), Havana, Cuba

⁸ Centro de Investigación y de Estudios Avanzados (CINVESTAV), Mexico City and Mérida, Mexico

⁹ Chicago State University, Chicago, Illinois, United States

¹⁰ China Institute of Atomic Energy, Beijing, China

¹¹ Chungbuk National University, Cheongju, Republic of Korea

¹² Comenius University Bratislava, Faculty of Mathematics, Physics and Informatics, Bratislava, Slovak Republic

¹³ COMSATS University Islamabad, Islamabad, Pakistan

¹⁴ Creighton University, Omaha, Nebraska, United States

¹⁵ Department of Physics, Aligarh Muslim University, Aligarh, India

¹⁶ Department of Physics, Pusan National University, Pusan, Republic of Korea

¹⁷ Department of Physics, Sejong University, Seoul, Republic of Korea

¹⁸ Department of Physics, University of California, Berkeley, California, United States

¹⁹ Department of Physics, University of Oslo, Oslo, Norway

²⁰ Department of Physics and Technology, University of Bergen, Bergen, Norway

²¹ Dipartimento di Fisica, Università di Pavia, Pavia, Italy

²² Dipartimento di Fisica dell'Università and Sezione INFN, Cagliari, Italy

²³ Dipartimento di Fisica dell'Università and Sezione INFN, Trieste, Italy

²⁴ Dipartimento di Fisica dell'Università and Sezione INFN, Turin, Italy

²⁵ Dipartimento di Fisica e Astronomia dell'Università and Sezione INFN, Bologna, Italy

²⁶ Dipartimento di Fisica e Astronomia dell'Università and Sezione INFN, Catania, Italy

²⁷ Dipartimento di Fisica e Astronomia dell'Università and Sezione INFN, Padova, Italy

²⁸ Dipartimento di Fisica 'E.R. Caianiello' dell'Università and Gruppo Collegato INFN, Salerno, Italy

²⁹ Dipartimento DISAT del Politecnico and Sezione INFN, Turin, Italy

³⁰ Dipartimento di Scienze MIFT, Università di Messina, Messina, Italy

³¹ Dipartimento Interateneo di Fisica 'M. Merlin' and Sezione INFN, Bari, Italy

³² European Organization for Nuclear Research (CERN), Geneva, Switzerland

³³ Faculty of Electrical Engineering, Mechanical Engineering and Naval Architecture, University of Split, Split, Croatia

³⁴ Faculty of Engineering and Science, Western Norway University of Applied Sciences, Bergen, Norway

³⁵ Faculty of Nuclear Sciences and Physical Engineering, Czech Technical University in Prague, Prague, Czech Republic

³⁶ Faculty of Physics, Sofia University, Sofia, Bulgaria

³⁷ Faculty of Science, P.J. Šafárik University, Košice, Slovak Republic

³⁸ Frankfurt Institute for Advanced Studies, Johann Wolfgang Goethe-Universität Frankfurt, Frankfurt, Germany

- ³⁹ Fudan University, Shanghai, China
⁴⁰ Gangneung-Wonju National University, Gangneung, Republic of Korea
⁴¹ Gauhati University, Department of Physics, Guwahati, India
⁴² Helmholtz-Institut für Strahlen- und Kernphysik, Rheinische Friedrich-Wilhelms-Universität Bonn, Bonn, Germany
⁴³ Helsinki Institute of Physics (HIP), Helsinki, Finland
⁴⁴ High Energy Physics Group, Universidad Autónoma de Puebla, Puebla, Mexico
⁴⁵ Horia Hulubei National Institute of Physics and Nuclear Engineering, Bucharest, Romania
⁴⁶ Indian Institute of Technology Bombay (IIT), Mumbai, India
⁴⁷ Indian Institute of Technology Indore, Indore, India
⁴⁸ INFN, Laboratori Nazionali di Frascati, Frascati, Italy
⁴⁹ INFN, Sezione di Bari, Bari, Italy
⁵⁰ INFN, Sezione di Bologna, Bologna, Italy
⁵¹ INFN, Sezione di Cagliari, Cagliari, Italy
⁵² INFN, Sezione di Catania, Catania, Italy
⁵³ INFN, Sezione di Padova, Padova, Italy
⁵⁴ INFN, Sezione di Pavia, Pavia, Italy
⁵⁵ INFN, Sezione di Torino, Turin, Italy
⁵⁶ INFN, Sezione di Trieste, Trieste, Italy
⁵⁷ Inha University, Incheon, Republic of Korea
⁵⁸ Institute for Gravitational and Subatomic Physics (GRASP), Utrecht University/Nikhef, Utrecht, Netherlands
⁵⁹ Institute of Experimental Physics, Slovak Academy of Sciences, Košice, Slovak Republic
⁶⁰ Institute of Physics, Homi Bhabha National Institute, Bhubaneswar, India
⁶¹ Institute of Physics of the Czech Academy of Sciences, Prague, Czech Republic
⁶² Institute of Space Science (ISS), Bucharest, Romania
⁶³ Institut für Kernphysik, Johann Wolfgang Goethe-Universität Frankfurt, Frankfurt, Germany
⁶⁴ Instituto de Ciencias Nucleares, Universidad Nacional Autónoma de México, Mexico City, Mexico
⁶⁵ Instituto de Física, Universidade Federal do Rio Grande do Sul (UFRGS), Porto Alegre, Brazil
⁶⁶ Instituto de Física, Universidad Nacional Autónoma de México, Mexico City, Mexico
⁶⁷ iThemba LABS, National Research Foundation, Somerset West, South Africa
⁶⁸ Jeonbuk National University, Jeonju, Republic of Korea
⁶⁹ Johann-Wolfgang-Goethe Universität Frankfurt Institut für Informatik, Fachbereich Informatik und Mathematik, Frankfurt, Germany
⁷⁰ Korea Institute of Science and Technology Information, Daejeon, Republic of Korea
⁷¹ KTO Karatay University, Konya, Turkey
⁷² Laboratoire de Physique des 2 Infinis, Irène Joliot-Curie, Orsay, France
⁷³ Laboratoire de Physique Subatomique et de Cosmologie, Université Grenoble-Alpes, CNRS-IN2P3, Grenoble, France
⁷⁴ Lawrence Berkeley National Laboratory, Berkeley, California, United States
⁷⁵ Lund University Department of Physics, Division of Particle Physics, Lund, Sweden
⁷⁶ Nagasaki Institute of Applied Science, Nagasaki, Japan
⁷⁷ Nara Women's University (NWU), Nara, Japan
⁷⁸ National and Kapodistrian University of Athens, School of Science, Department of Physics, Athens, Greece
⁷⁹ National Centre for Nuclear Research, Warsaw, Poland
⁸⁰ National Institute of Science Education and Research, Homi Bhabha National Institute, Jatni, India
⁸¹ National Nuclear Research Center, Baku, Azerbaijan
⁸² National Research and Innovation Agency - BRIN, Jakarta, Indonesia
⁸³ Niels Bohr Institute, University of Copenhagen, Copenhagen, Denmark
⁸⁴ Nikhef, National institute for subatomic physics, Amsterdam, Netherlands
⁸⁵ Nuclear Physics Group, STFC Daresbury Laboratory, Daresbury, United Kingdom
⁸⁶ Nuclear Physics Institute of the Czech Academy of Sciences, Husinec-Řež, Czech Republic
⁸⁷ Oak Ridge National Laboratory, Oak Ridge, Tennessee, United States
⁸⁸ Ohio State University, Columbus, Ohio, United States
⁸⁹ Physics department, Faculty of science, University of Zagreb, Zagreb, Croatia
⁹⁰ Physics Department, Panjab University, Chandigarh, India
⁹¹ Physics Department, University of Jammu, Jammu, India

- ⁹² Physics Program and International Institute for Sustainability with Knotted Chiral Meta Matter (SKCM2), Hiroshima University, Hiroshima, Japan
- ⁹³ Physikalisches Institut, Eberhard-Karls-Universität Tübingen, Tübingen, Germany
- ⁹⁴ Physikalisches Institut, Ruprecht-Karls-Universität Heidelberg, Heidelberg, Germany
- ⁹⁵ Physik Department, Technische Universität München, Munich, Germany
- ⁹⁶ Politecnico di Bari and Sezione INFN, Bari, Italy
- ⁹⁷ Research Division and ExtreMe Matter Institute EMMI, GSI Helmholtzzentrum für Schwerionenforschung GmbH, Darmstadt, Germany
- ⁹⁸ Saga University, Saga, Japan
- ⁹⁹ Saha Institute of Nuclear Physics, Homi Bhabha National Institute, Kolkata, India
- ¹⁰⁰ School of Physics and Astronomy, University of Birmingham, Birmingham, United Kingdom
- ¹⁰¹ Sección Física, Departamento de Ciencias, Pontificia Universidad Católica del Perú, Lima, Peru
- ¹⁰² Stefan Meyer Institut für Subatomare Physik (SMI), Vienna, Austria
- ¹⁰³ SUBATECH, IMT Atlantique, Nantes Université, CNRS-IN2P3, Nantes, France
- ¹⁰⁴ Sungkyunkwan University, Suwon City, Republic of Korea
- ¹⁰⁵ Suranaree University of Technology, Nakhon Ratchasima, Thailand
- ¹⁰⁶ Technical University of Košice, Košice, Slovak Republic
- ¹⁰⁷ The Henryk Niewodniczanski Institute of Nuclear Physics, Polish Academy of Sciences, Cracow, Poland
- ¹⁰⁸ The University of Texas at Austin, Austin, Texas, United States
- ¹⁰⁹ Universidad Autónoma de Sinaloa, Culiacán, Mexico
- ¹¹⁰ Universidade de São Paulo (USP), São Paulo, Brazil
- ¹¹¹ Universidade Estadual de Campinas (UNICAMP), Campinas, Brazil
- ¹¹² Universidade Federal do ABC, Santo Andre, Brazil
- ¹¹³ University of Cape Town, Cape Town, South Africa
- ¹¹⁴ University of Houston, Houston, Texas, United States
- ¹¹⁵ University of Jyväskylä, Jyväskylä, Finland
- ¹¹⁶ University of Kansas, Lawrence, Kansas, United States
- ¹¹⁷ University of Liverpool, Liverpool, United Kingdom
- ¹¹⁸ University of Science and Technology of China, Hefei, China
- ¹¹⁹ University of South-Eastern Norway, Kongsberg, Norway
- ¹²⁰ University of Tennessee, Knoxville, Tennessee, United States
- ¹²¹ University of the Witwatersrand, Johannesburg, South Africa
- ¹²² University of Tokyo, Tokyo, Japan
- ¹²³ University of Tsukuba, Tsukuba, Japan
- ¹²⁴ University Politehnica of Bucharest, Bucharest, Romania
- ¹²⁵ Université Clermont Auvergne, CNRS/IN2P3, LPC, Clermont-Ferrand, France
- ¹²⁶ Université de Lyon, CNRS/IN2P3, Institut de Physique des 2 Infinis de Lyon, Lyon, France
- ¹²⁷ Université de Strasbourg, CNRS, IPHC UMR 7178, F-67000 Strasbourg, France, Strasbourg, France
- ¹²⁸ Université Paris-Saclay Centre d'Etudes de Saclay (CEA), IRFU, Département de Physique Nucléaire (DPhN), Saclay, France
- ¹²⁹ Università degli Studi di Foggia, Foggia, Italy
- ¹³⁰ Università del Piemonte Orientale, Vercelli, Italy
- ¹³¹ Università di Brescia, Brescia, Italy
- ¹³² Variable Energy Cyclotron Centre, Homi Bhabha National Institute, Kolkata, India
- ¹³³ Warsaw University of Technology, Warsaw, Poland
- ¹³⁴ Wayne State University, Detroit, Michigan, United States
- ¹³⁵ Westfälische Wilhelms-Universität Münster, Institut für Kernphysik, Münster, Germany
- ¹³⁶ Wigner Research Centre for Physics, Budapest, Hungary
- ¹³⁷ Yale University, New Haven, Connecticut, United States
- ¹³⁸ Yonsei University, Seoul, Republic of Korea
- ¹³⁹ Zentrum für Technologie und Transfer (ZTT), Worms, Germany
- ¹⁴⁰ Affiliated with an institute covered by a cooperation agreement with CERN
- ¹⁴¹ Affiliated with an international laboratory covered by a cooperation agreement with CERN.